Gob and Gate Road Reaction to Longwall Mining in Bump-Prone Strata

By Alan A. Campoli, Timothy M. Barton, Fred C. Van Dyke, and Michael Gauna

UNITED STATES DEPARTMENT OF THE INTERIOR

BUREAU OF MINES

Mission: As the Nation's principal conservation agency, the Department of the Interior has responsibility for most of our nationally-owned public lands and natural and cultural resources. This includes fostering wise use of our land and water resources, protecting our fish and wildlife, preserving the environmental and cultural values of our national parks and historical places, and providing for the enjoyment of life through outdoor recreation. The Department assesses our energy and mineral resources and works to assure that their development is in the best interests of all our people. The Department also promotes the goals of the Take Pride in America campaign by encouraging stewardship and citizen responsibility for the public lands and promoting citizen participation in their care. The Department also has a major responsibility for American Indian reservation communities and for people who live in Island Territories under U.S. Administration.

Report of Investigations 9445

Gob and Gate Road Reaction to Longwall Mining in Bump-Prone Strata

By Alan A. Campoli, Timothy M. Barton, Fred C. Van Dyke, and Michael Gauna

UNITED STATES DEPARTMENT OF THE INTERIOR

BUREAU OF MINES

Library of Congress Cataloging in Publication Data:

Gob and gate road reaction to longwall mining in bump-prone strata / by Alan A. Campoli...[et al.].

p. cm. — (Report of investigations; 9445)

Includes bibliographical references (p. 48).

1. Mine roof control. 2. Rock bursts. 3. Longwall mining. I. Campoli, A. A. (Alan A.). II. Series: Report of investigations (United States. Bureau of Mines); 9445.

TN23.U43 [TN288] 622 s—dc20 [622'.334] 92-23264 CIP

CONTENTS

ILLUSTRATIONS

ILLUSTRATIONS—Continued

TABLES

UNIT OF MEASURE ABBREVIATIONS USED IN THIS REPORT

ft	foot	psi	pound (force) per square inch
h	hour	s	second
hp	horsepower	V ac	volt, alternating current
in	inch	V dc	volt, direct current
in/in	inch per inch (strain)		

GOB AND GATE ROAD REACTION TO LONGWALL MINING IN BUMP-PRONE STRATA

By Alan A. Campoli,[1] Timothy M. Barton,[1] Fred C. Van Dyke,[2] and Michael Gauna[3]

ABSTRACT

The U.S. Bureau of Mines conducted research to characterize longwall gob loading under bump-prone geologic conditions. Bureau-designed stress meters were installed in the floor rock beneath two longwall panels and coal pillars in the gate road between them. Gob and gate road pillar stress was monitored continuously by a state-of-the-art data acquisition system. The timing of the final destruction of the abutment pillar's load-bearing core was optimal, since the pillar is located between two gob areas and no longer of significant importance for ground control. Maximum stress was observed immediately in front of the longwall face, and this pressure quickly dropped as the face moved past the instruments. The center of the longwall panels regained significant overburden load, while the instruments located less than 100 ft from the edge of the panel showed little or no increase in pressure due to gob reloading.

[1]Mining engineer, Pittsburgh Research Center, U.S. Bureau of Mines, Pittsburgh, PA.
[2]Mining engineering technician, Pittsburgh Research Center.
[3]Manager of planning engineering, Island Creek Coal Co., Oakwood, VA.

INTRODUCTION

The retreat longwall coal mining method redistributes the weight of the overburden among the longwall face, active gob, gate road pillars, and adjacent unmined panel. The pattern of stress redistribution is influenced by the geologic setting. A previous U.S. Bureau of Mines field study in a Virginia coal mine in the Pocahontas No. 3 Coalbed documented a gate road designed to alleviate the risk of coal mine bumps on retreat longwall sections (*3*).[4] As part of the Bureau's program to develop technology to reduce accidents due to coal mine bumps, research was conducted to characterize longwall gob loading under bump-prone geologic conditions. A coal mine bump is the massive release of energy associated with the violent failure of coal due to overstress. During retreat room-and-pillar and longwall mining, redistributed stresses are concentrated directly outby gob areas. This becomes critical when mining is conducted where the coalbed is encased in rigid associated strata. Unbroken overlying strata over adjoining gob areas transfer pressure onto adjacent pillars and unmined areas where this additional pressure causes the threat of coal bumps. Coal mine bumps have caused 14 fatalities from 1959 to 1987 in the Eastern States of Kentucky, West Virginia, Pennsylvania, and Virginia (*15*). The occurrence of numerous bumps at four coal mines in Virginia and Kentucky in the past 2 years emphasizes the continuing need for appropriate design guidelines in bump-prone ground.

The Southern Appalachian Basin of the United States has had a long history of coal bumps and coal bump research. The Bureau published one of the earliest detailed reports about coal bumps in this area. Compiled by Rice (*22*), this report identified numerous sites of coal pillar bumps in eastern Kentucky and southwestern Virginia and noted that in one 4-month period, eight miners were killed and a number injured by bumps. In another report, Holland and Thomas (*11*) examined 177 instances of pillar bumps, most of which were in the Southern Appalachian Basin, and found that the primary cause of these bumps was "unfavorable" mining practices in abutment areas. Talman and Schroder (*23*) noted the importance of very stiff overlying strata to the occurrence of bumps, thereby emphasizing the influence of local geologic conditions. Comprehensive laboratory and field data on the physical properties of two bump-prone coals from Southern Appalachia (Pocahontas No. 3 and 4 Coalbeds) were reported by Wang, Skelly, and Wolgamott (*25*). No characteristics of these coalbeds indicated a particular preference for them to bump.

Bureau coal mine bump research continued in the Southern Appalachian Basin after the occurrence of a rash of bump-related fatalities and injuries in 1984 and 1985 (*5*). A preliminary investigation of the geologic, mining, and engineering parameters at five sites in West Virginia and Virginia, where recent miner fatalities or injuries were associated with coal bumps, revealed that stiff, competent associated strata and the high stresses generated by retreat mining were common to all five sites. These findings supported the earlier conclusion of Holland and Thomas (*11*) that the probability of bump occurrence is increased by certain mining practices that concentrate stresses during retreat mining. This preliminary report recommended that the development of pillar line points or long roof spans that propagate bumps should be avoided in mine designs. Also, retreating longwalls with carefully designed gate roads were recommended over room-and-pillar retreat in deep bump-prone mines (*5*).

The Bureau's bump research program initiated the development of design criteria for controlling bumps with an inmine evaluation of a novel extraction sequence used to control bumps during room-and-pillar retreat coal mining at the Olga Mine, McDowell County, WV. This novel retreat mining system, which conducted mining over three pillar rows outby the gob, distributed abutment loads up to six pillar rows outby the newly formed gob. Microseismic monitoring was also conducted in the Olga Mine study area; the results of this effort were reported by Condon and Munson (*7*).

Using roof-to-floor convergence and coalbed pressure measurements, many facets of bump-prone strata were investigated at this site. Maximum strain energy storage in the chain pillars occurred just prior to the first of four chain pillar split cuts. Before these split cuts, a 15-ft-wide yielded perimeter confined the core of the 55- by 70-ft pillars, permitting the soft coalbed to support tremendous loads. Splitting the chain pillars into two 17.5- by 70-ft wings removed the confining pressure. From convergence and stress measurements it was apparent that structural failure of the pillar occurred after the third pillar split cut. Thus, by strategically softening pillars in the abutment zone, the novel mining method successfully redistributed dangerous strain energy away from the pillar line (*15*).

Shot fire and auger drilling distressing techniques were also evaluated at this mine. Both techniques induced instantaneous roof-to-floor convergence, indicating a softening of the subject chain pillars. This resulted in a reduction of the energy storage capacity of the pillars. Both roof-to-floor convergence and cuttings volume measurement indicated that the drilling of 4-in auger boreholes was effective for stress reduction on highly stressed pillars. Thus, both localized distressing techniques enhanced the effectiveness of the mining method in redistributing strain energy (*6*).

[4]Italic numbers in parentheses refer to items in the list of references at the end of this report.

The goal of the current research program is to develop a design criterion that can be used to minimize the bump hazard of mining layouts (*4*). The foundation of this program is the delineation of the detailed reactions and physical properties of the bump-prone coal strata through inmine evaluations. The results of the Olga Mine study were enhanced by an evaluation of two different bump-control longwall gate road configurations in a deep bump-prone coal mine in the Southern Appalachian Basin, namely the VP No. 3 Mine of Island Creek Coal Co. in Vansant, VA (*14*). The first gate road studied employed a yield-abutment-yield configuration with the yield pillars on 50-ft centers, abutment pillars on 100-ft centers, and all crosscuts on 100-ft centers. In this earlier design, an 80-ft-square pillar was adjacent to the panel tailgate. This pillar frequently experienced heavy bumps directly adjacent to the tail drive, causing coal to be thrown into the face area (*5*). However, in the yield-abutment-yield design, the 80- by 30-ft outside yield pillars essentially yielded on the headgate pass of the face, thereby eliminating their potential to bump. The yielded pillars effectively shield workers from coal thrown in the event that the 80-ft-square abutment pillars bump during the subsequent tailgate pass.

This technique of shielding the workers from the potential abutment pillar bumps on the tailgate side of the panel is satisfactory if the abutment pillar bumps occur behind the longwall face or adjacent to the tail drive. However, when mining expanded under deeper cover, the tail-side abutment pillars began bumping in advance of the face. In the first gate road studied, bumps of this nature completely closed the 20-ft-wide crosscuts between the tail-side abutment pillars (*13*). Also, when the tailgate abutment pillars started failing outby the tail drive, bumps began to occur directly on the longwall face.

In an attempt to control the tailgate bumps and to standardize their gate road design, the mine operator switched to an alternate yield-abutment-yield configuration in the second gate road studied. This latest design consists of yield pillars on 40-ft centers and abutment pillars on 140-ft centers. Between the yield pillars, the crosscuts were driven at 60° angles on 100-ft centers, whereas between the abutment pillars the crosscuts were driven at 90° angles on 200-ft centers. This layout results in 20- by 80-ft yield pillars on either side of a center 120- by 180-ft abutment pillar. Pillar stress measurements, within the soft, friable Pocahontas No. 3 Coalbed, were successfully obtained with the stainless steel borehole platened flatjack (BPF) (*10*). The larger abutment pillars in this new design carried the applied abutment loads and thus prevented the ground stresses from overriding onto the longwall face (*3*). While pillar behavior was similar, the design change did significantly increase the effective life of the 120-ft-wide abutment pillars. The design change delayed abutment pillar bumps from 500 ft in advance of the face to 100 ft behind the face and greatly diminished bump intensity and eliminated face bumps (*2*).

This report documents a field project specifically designed to characterize the longwall gob behavior at the VP No. 3 Mine. The overall goal was to obtain an understanding of the far-field loading mechanism in the unique bump-prone strata of Southern Appalachia and to build upon the stress and deformation data base. The accumulated knowledge base resulting from these research efforts will be utilized in the development of bump control and mine design procedures. The proposed design methodology will primarily be implemented through the numerical model MULSIM/NL (*9*). This program, which is based on the displacement discontinuity method, can be used to produce models of mining-induced stress, displacements, and energy values. If the model is to be realistic and practical, it must be calibrated with actual field data. One of the major problems with previous models has been the evaluation and calibration of the gob load because the correct material properties were not available and only minimal gob pressure readings were available for calibration.

ACKNOWLEDGMENTS

This work could not have been accomplished without the help of the following Island Creek Coal Co. employees from the Virginia Pocahontas Div., Oakwood, VA: Kenneth R. Price, general manager; Rufus Fox, operations manager; Eddie Ball, mine superintendent; and Howard Epperly, manager of engineering. They provided the valued information, insight, advice, and inmine assistance that made this publication possible.

ABUTMENT LOADING IN FULL EXTRACTION ENVIRONMENT

Retreat longwall coal mining is performed in two distinct stages: Gate road development with continuous miner sections precedes panel extraction by longwall methods. Prior to gate road development, the weight of the overburden is uniformly distributed over the coalbed by the relatively stronger roof and floor rocks. Gate road

development disrupts the original equilibrium conditions. However, the sum total of the weight of the overburden remains unchanged. Potential energy balance requires that the stress distribution in the area has to be readjusted so that a new equilibrium state can be achieved. The weight of the overburden carried by the coal removed during gate road development is transferred to the surrounding gate road pillars and adjacent longwall panels. The transferred vertical stress concentrates in the perimeters of the gate road pillars and adjacent panels. These zones of stress concentration are called abutments and the pressures in excess of the in situ vertical stress are called abutment pressures.

The energy balance is further upset by the mining of the longwall panel. Figure 1 [after Peng and Chiang (*21*)] idealizes the new equilibrium state achieved when the weight of the overburden carried by the mined coal is redistributed among the longwall face, active gob, gate road pillars, and adjacent unmined panels. Local stress concentrations within the gate road pillars are not shown to illustrate general trends in vertical stress in and around the retreat longwall panel. The stress concentration in advance of the face is called the front abutment pressure. Wilson (*27*) estimates that the front abutment peak value is somewhere between three and five times the cover load alongside wide excavations. The front abutment pressure is the result of stress being concentrated at or near the active longwall face. It is generally thought that the load carried by the gob floor increases with the distance away from the active face, until it is slightly less than and asymptotic to the original in situ vertical pressure [figure 2, section CC' (after Peng and Chiang (*21*))]. The weight on the sides of the longwall panel are termed the headgate and tailgate side abutment pressures (figure 2, section RR'). The front and side abutments intersect at the corners of the panel and their stresses are superimposed on each other. Both the front and side abutment pressures decrease exponentially away from the edges of the mined panel and return to the overburden pressure some distance away from the mined panel. Side abutment pressure near the ribs of the headgate and tailgate begins to increase when the face is some distance inby. It increases continuously and reaches the maximum value when the face has passed; thereafter, it stabilizes, although in some cases yielding occurs (figure 2, section SS').

Empirical and theoretical models have been developed to predict the way longwall abutment loads are shared

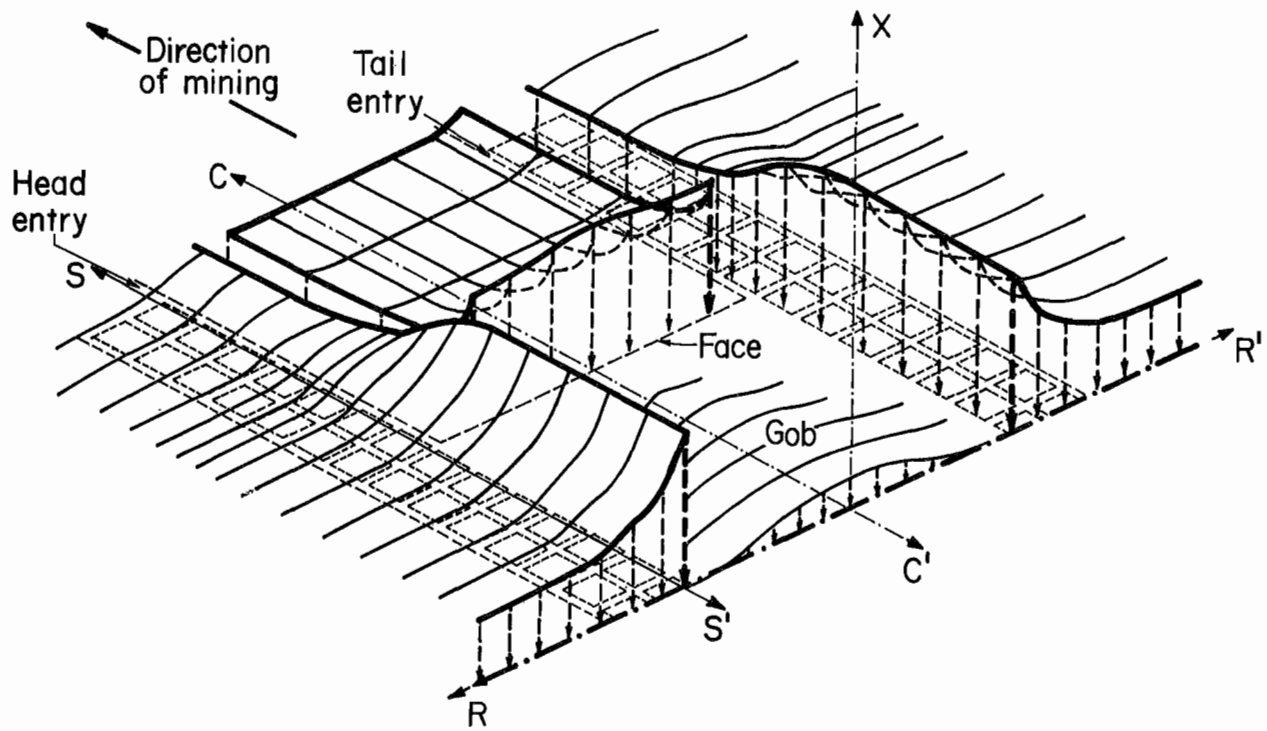

Figure 1.—Idealized three-dimensional representation of vertical stress around longwall panel. [From Peng and Chiang (*21*)].

among the gate road pillars, adjacent longwall panels, and gob. Wilson (*26*) theorized that vertical stress is redistributed linearly across the active gob with zero stress at its edge to original cover pressure at some distance within the gob and that distance to be 0.3 times the overburden depth. The weight of this load deficiency wedge is the side abutment load carried by the gate road. King and Whittaker (*16*) define this load deficiency wedge in terms of shear angle predictions from British subsidence conditions. Mark (*18*) incorporated an abutment angle of 21° in his estimation of side abutment loading for the analysis of longwall pillar stability (ALPS) method. This method was built on the measurement of abutment stresses on 16 longwall panels. Some researchers have used three-dimensional numerical models to solve this complicated potential energy balance calculation (*12*, *17*, *20*).

Field measurements of gob loading during full extraction have been conducted under varying sets of mining method and geological conditions. Oyanguren (*19*) described the use of subsidence monitoring, combined with rigid inclusion cells, and goaf load cells to measure longwall gob loading in the Esparza Potash Mine in Navarra, Spain. He reported a good correlation between the increase in vertical stress on the gob floor and the surface subsidence. Oyanguren reached the conclusion that at a distance of about 0.9 times the depth of overburden behind the face, the ground above the longwall gob was stabilized and the pressure on the gob floor had reached overburden pressure. This was not sensitive to changes in overburden thickness, which ranged from 600 to 1,200 ft.

Longwall coal gob behavior in the 700-ft-deep F Coalbed at the Eagle No. 5 Mine near Moffat, CO, was

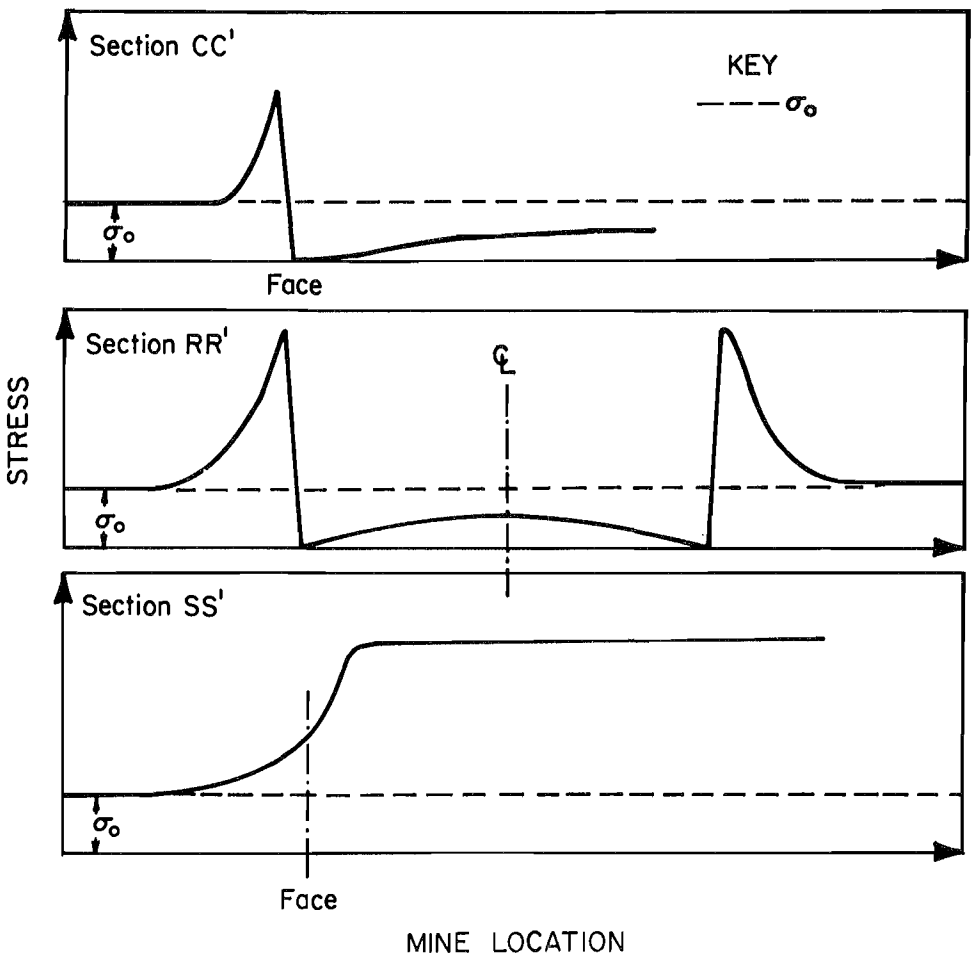

Figure 2.—Cross-section views of idealized vertical stress diagram. Sections are shown in figure 1. (σ_0 = original cover stress.) [From Peng and Chiang (*21*)].

recently investigated.[5] Their borehole pressure cells (*1*) showed a return to full overburden pressure at approximately 80 ft (0.113 times the depth of overburden) from the gob edge, much closer than predicted by Wilson's linear approximation. The immediate roof was composed of carbonaceous shale. The main roof was a nonhomogeneous section of interbedded sandstone, shale, and coal. These conditions are radically different from the massive sandstone formations encountered in bump-prone ground.

Wade and Conroy (*24*) investigated coal gob behavior in the Herrin No. 6 Coalbed at the Old Ben No. 24 Mine near Benton, IL. Vibrating wire stress meters were installed in and below a 600-ft-deep, 460- by 1,735-ft longwall panel, with a coalbed thickness of 96 to 104 in. Surface subsidence movements were correlated with underground stress data (fig. 3). Conroy reported[6] that front abutment pressures began 200 ft in advance of the face, the rate accelerated at approximately 100 ft in advance of the face, and peaked at 10 ft in advance of the face. The gob pres-sure was estimated to recover to the original overburden pressure 200 ft (0.3 times the depth of overburden) behind the face, and the gob had stabilized at a distance 500 ft behind the face (fig. 4). The immediate roof consisted of gray and black carbonaceous shales; thin beds of conglomerate, fossilferous limestone; and coal. The immediate bottom was 3 to 5 ft of soft gray claystone mixed with siltstone, over a light-gray, fine-grained limestone member. The main roof consisted of shale mixed with limestone beds. These conditions are quite different from the bump-prone conditions under which this study was conducted.

[5]A Bureau report is in progress; for further information, contact Donna Boreck, Denver Research Center, Denver, CO.

[6]Work done by Dames and Moore under Bureau of Mines contract J0333949.

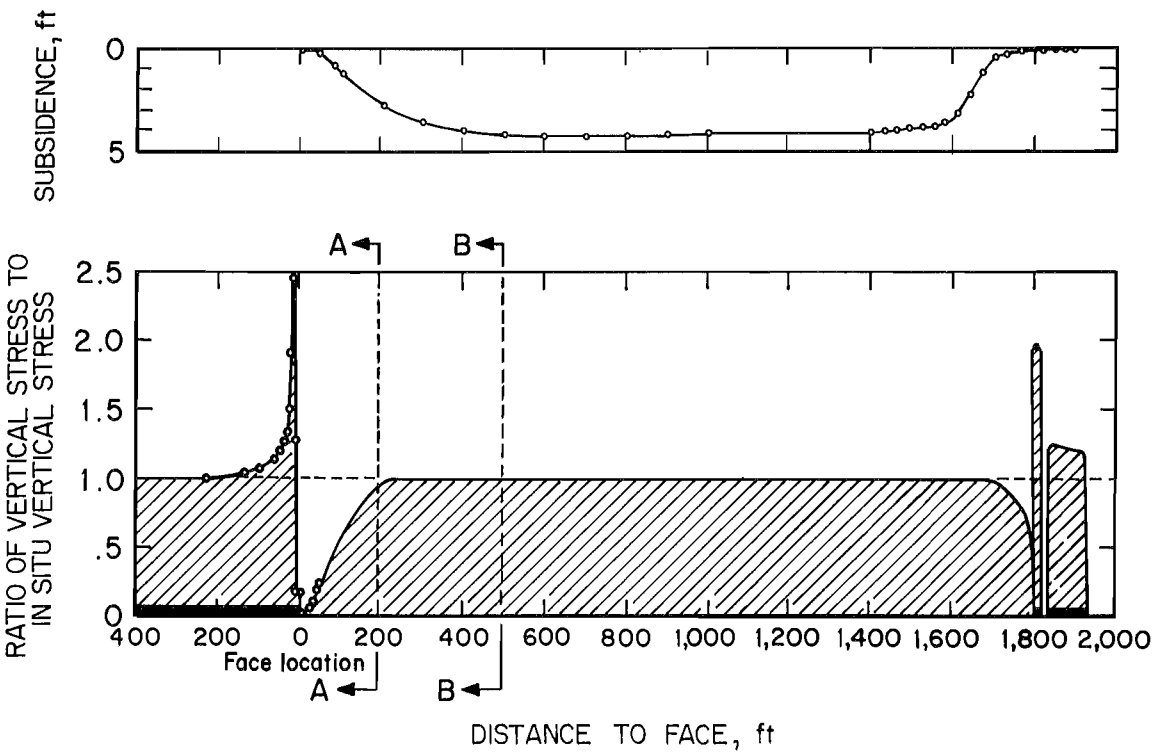

Figure 3.—Generalized vertical stress distribution and subsidence along panel center line.

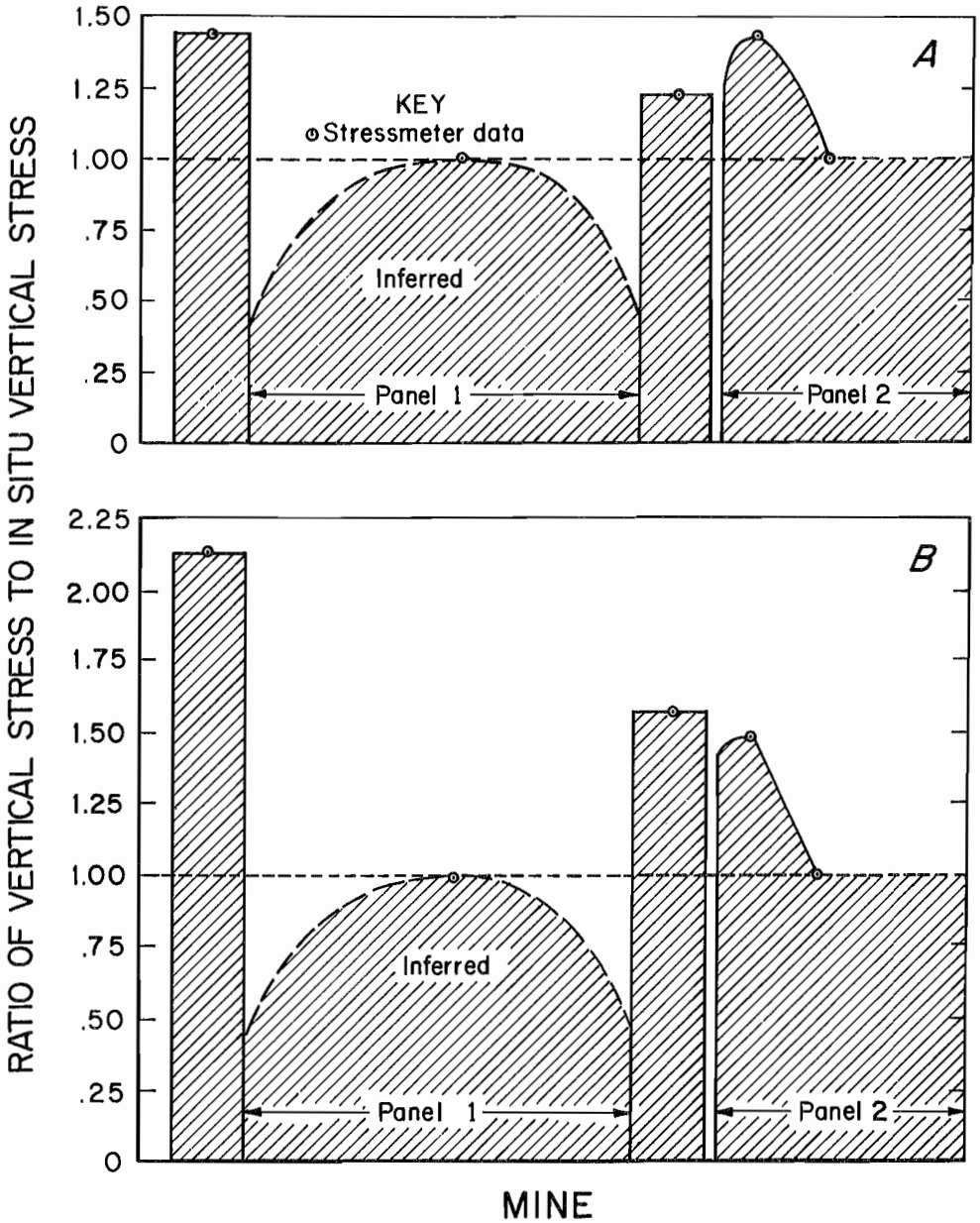

Figure 4.—Cross-section view of vertical stress distribution across two longwall panels. *A*, 200 ft from face; *B*, 500 ft from face. (Dashed line indicates original cover stress.)

GEOGRAPHIC AND GEOLOGIC SETTINGS

The study area is located in Buchanan County, VA (fig. 5). A total of 18 longwall panels have been mined from the subject mine (fig. 6). Eight successive panels have been mined to the north and 10 successive panels have been mined to the south of twin barrier pillars. The gate-entry system between the 9th and 10th panels to the south contained what will be referred to as the 10 development study area. It was the last of three detailed instrument arrays all established by the Bureau; these three locations are indicated in figure 6.

The mine operator extracts the Pocahontas No. 3 Coalbed, which is located in the Pocahontas Formation and averages 5.5 ft in thickness (fig. 7). Mine-wide, the Pocahontas No. 3 Coalbed is under overburden ranging from 1,200 to 2,200 ft in thickness (fig. 8) and the coalbed dips 1° from east to west (fig. 9). The immediate roof, in the south end of the mine, consists of a widely jointed siltstone overlain by a very stiff, massive sandstone. Mine-wide, the siltstone ranges from a maximum thickness of 110 ft down to being nonexistent (fig. 10). The massive sandstone in the main roof varies from a maximum thickness of 450 ft to a minimum of 135 ft (fig. 11). The mine floor, in the south end of the mine, consists of a combination of very competent siltstone and sandstone.

A section of the mine map showing the 10 development gate-entry system is presented in figure 12. All of the gate-entry pillar systems in this mine are of a conventional design. Conventional pillar designs are intended to support a major portion of abutment load resulting from adjacent gob formation. This is in contrast to an all-yield design that immediately transfers abutment load to the longwall panel during adjacent panel mining. Figure 12 also displays the variations in the overburden, siltstone immediate roof, and sandstone main roof thicknesses directly above the 10 development gate-entry system. The S-9 and S-10 panels are roughly 600 ft wide and 6,000 ft long.

Underground observations in the study areas (fig. 8), reported by Iannacchione (*14*), indicate a persistent absence of prominent roof and floor fractures or joints and that the main roof, dominated by the thick sandstone, is exceedingly difficult to break. These unique geologic conditions apparently cause greater pillar loads in the study area than would be predicted by conventional, empirical abutment load calculations, such as those proposed by Mark (*18*).

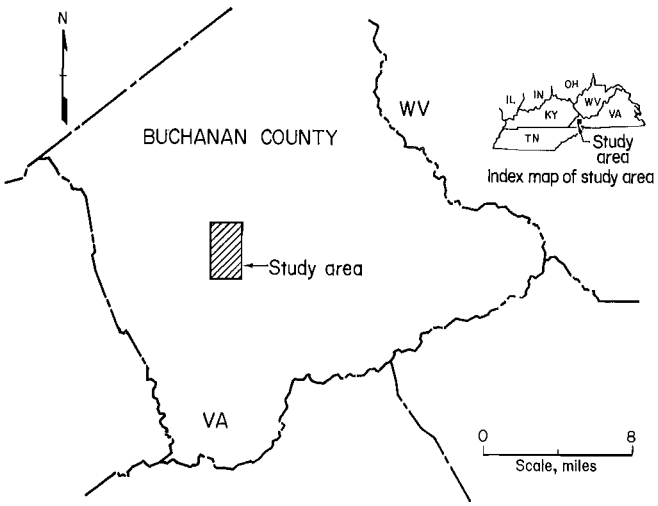

Figure 5.—Study area location map.

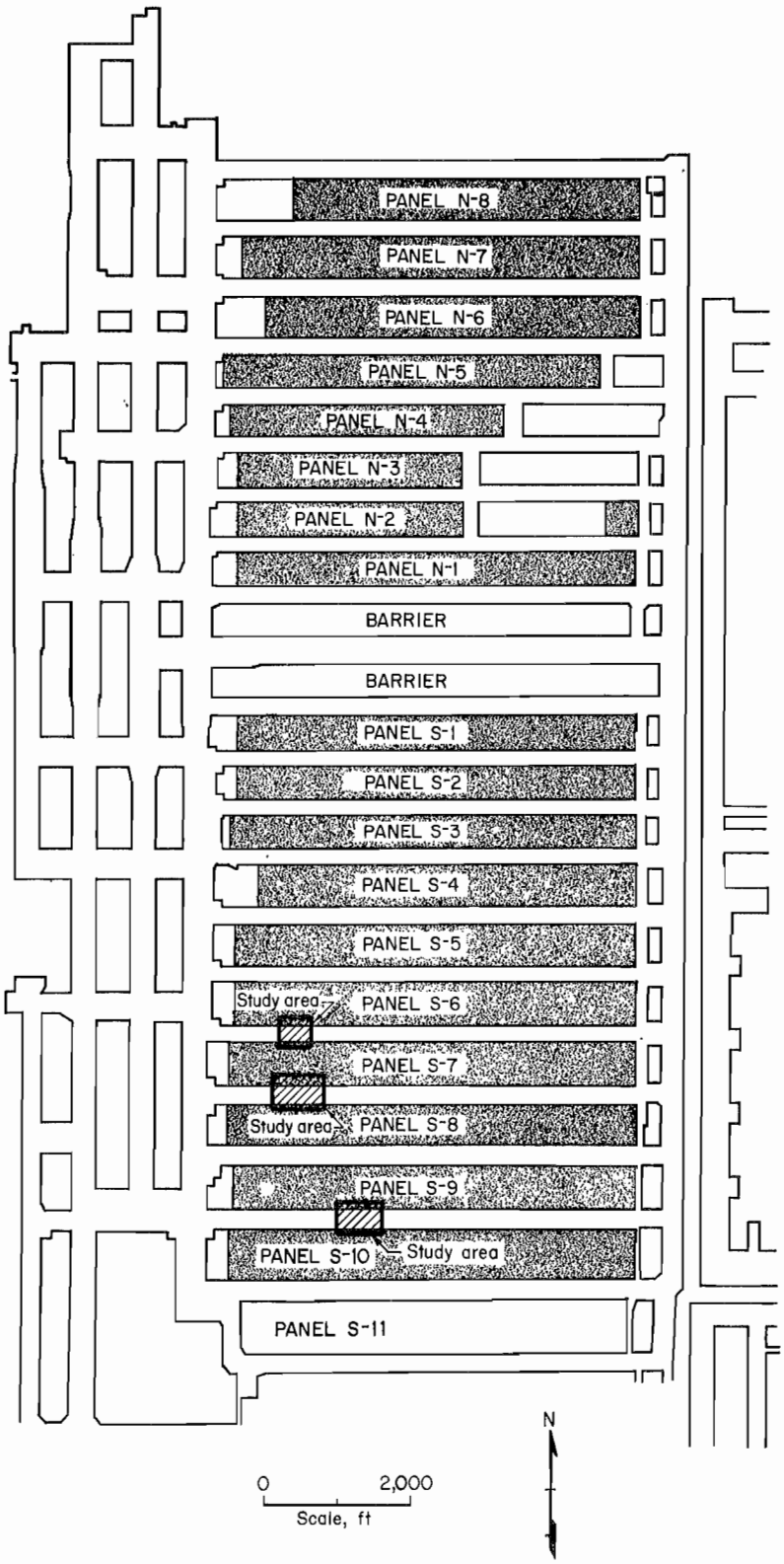

Figure 6.—Mine map.

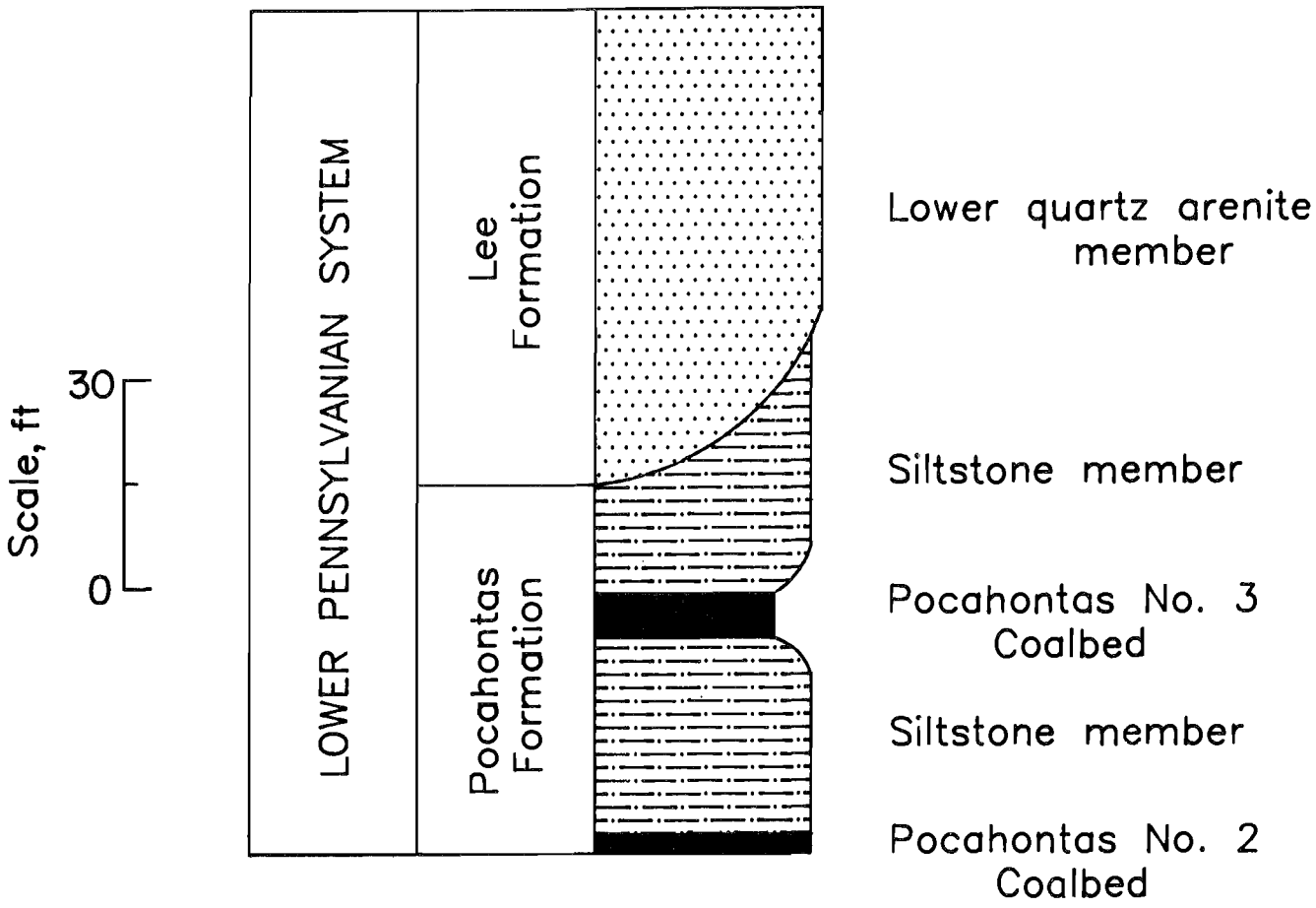

Figure 7.—Generalized stratigraphic column.

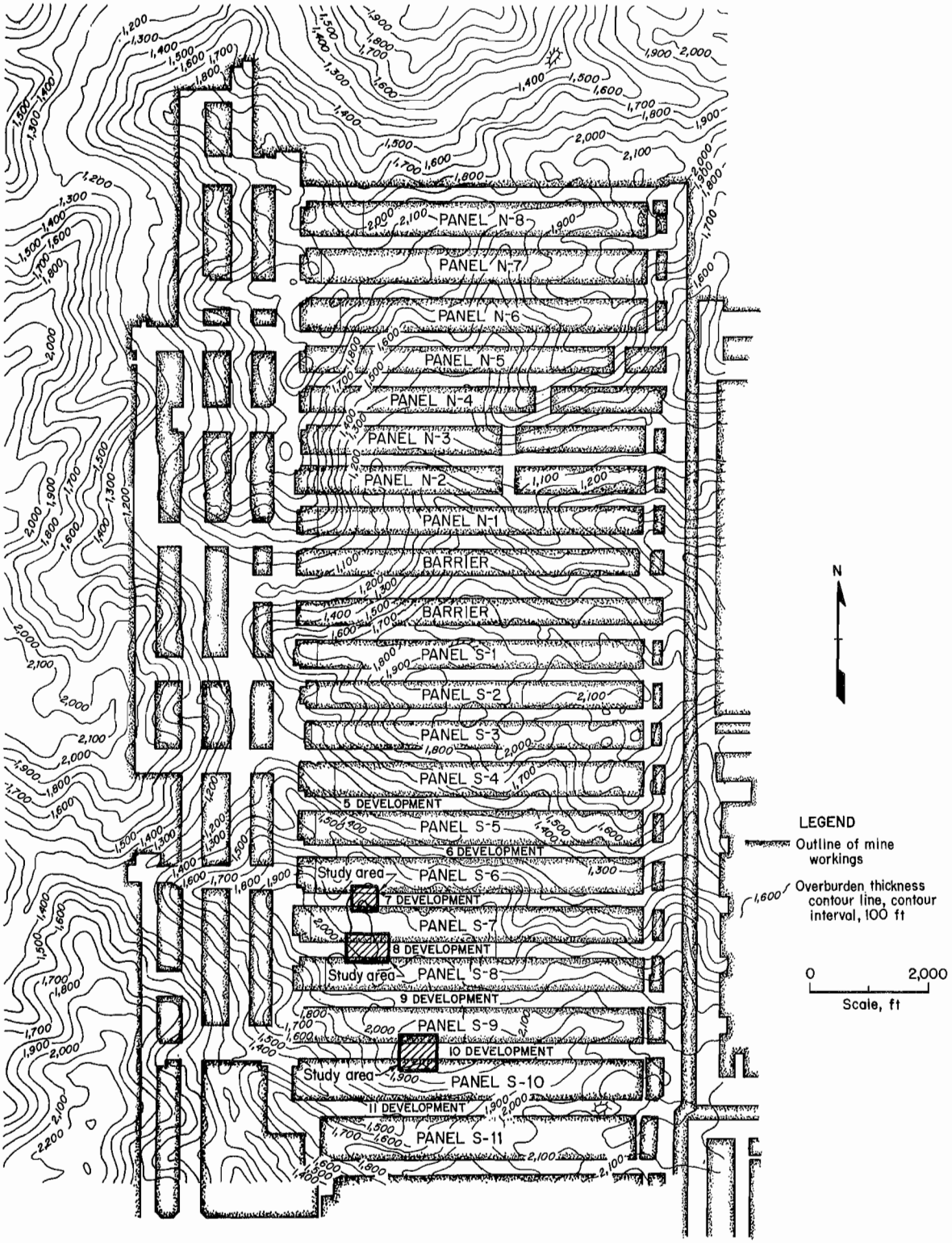

Figure 8.—Overburden map for Pocahontas No. 3 Coalbed.

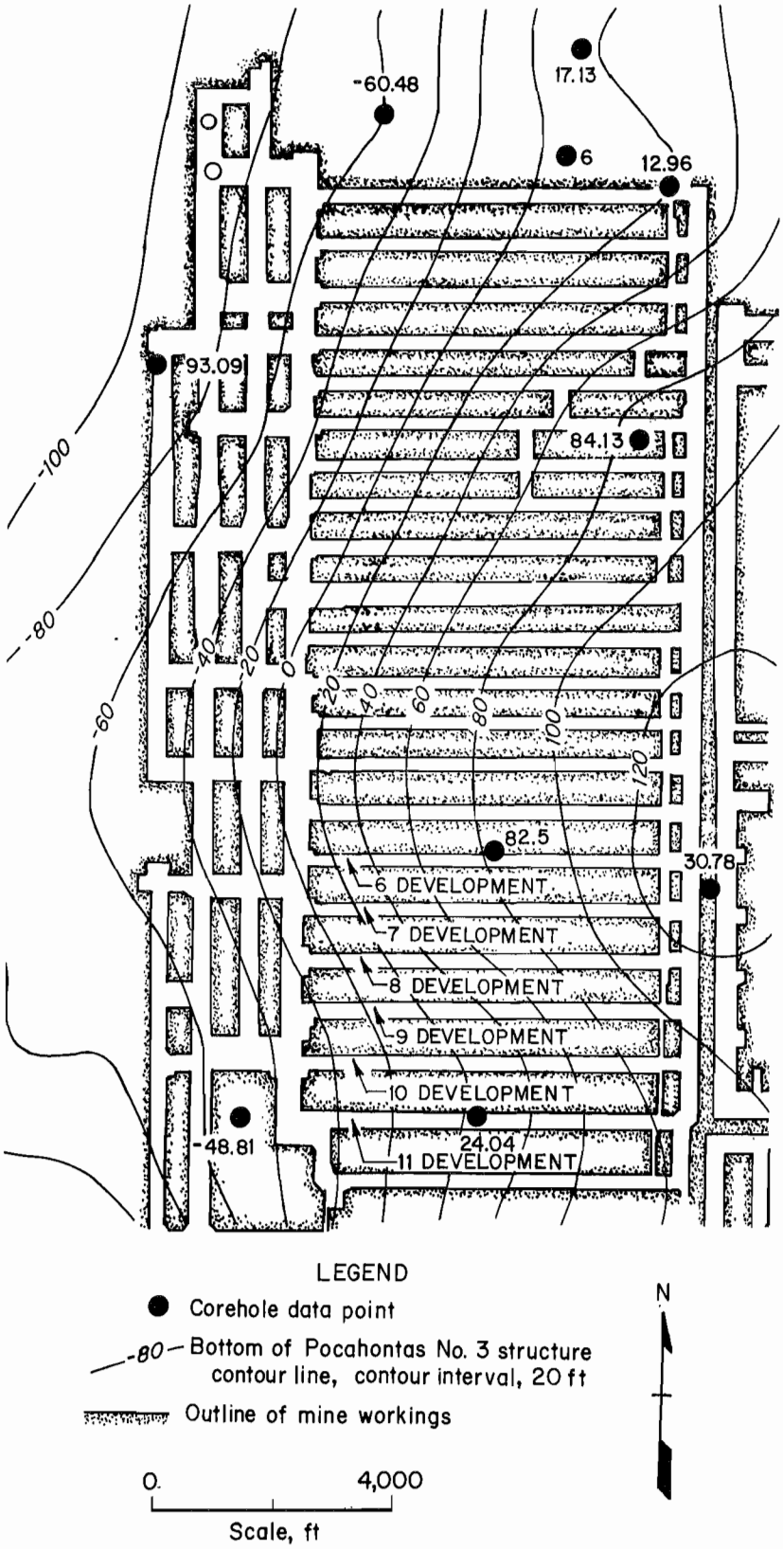

Figure 9.—Structure contour map on base of Pocahontas No. 3 Coalbed.

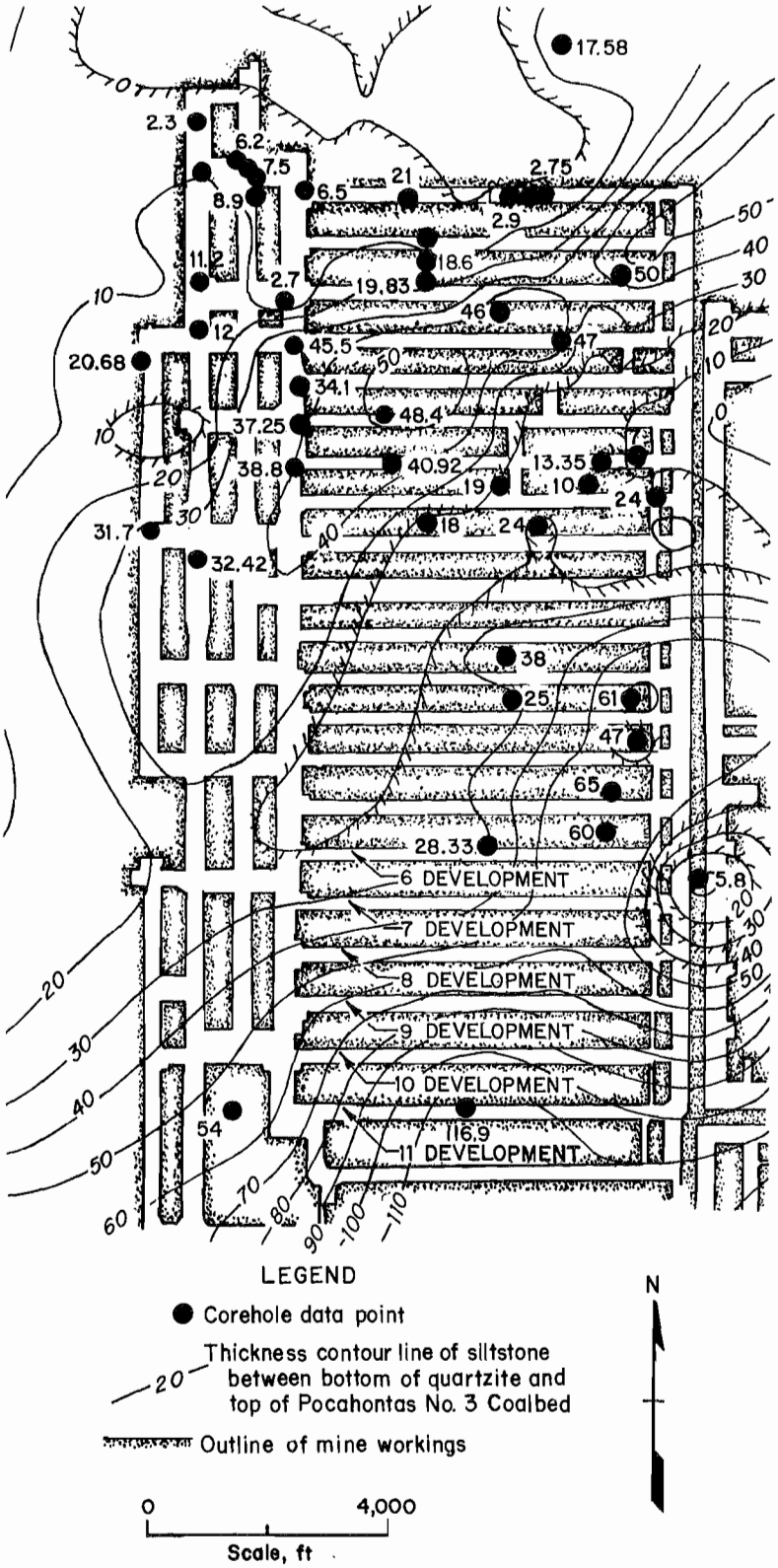

Figure 10.—Map of siltstone immediate roof thickness.

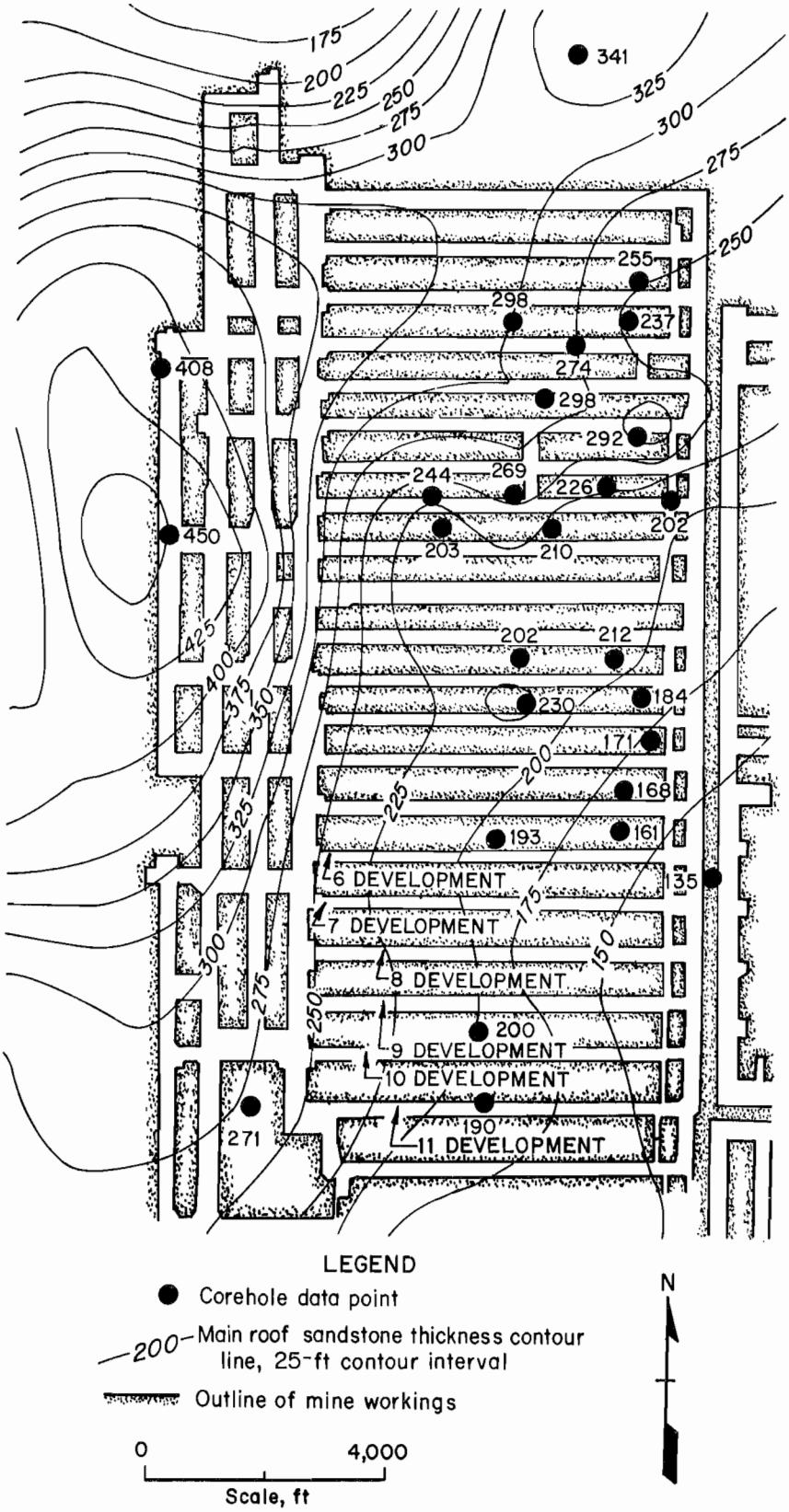

Figure 11.—Map of sandstone main roof thickness.

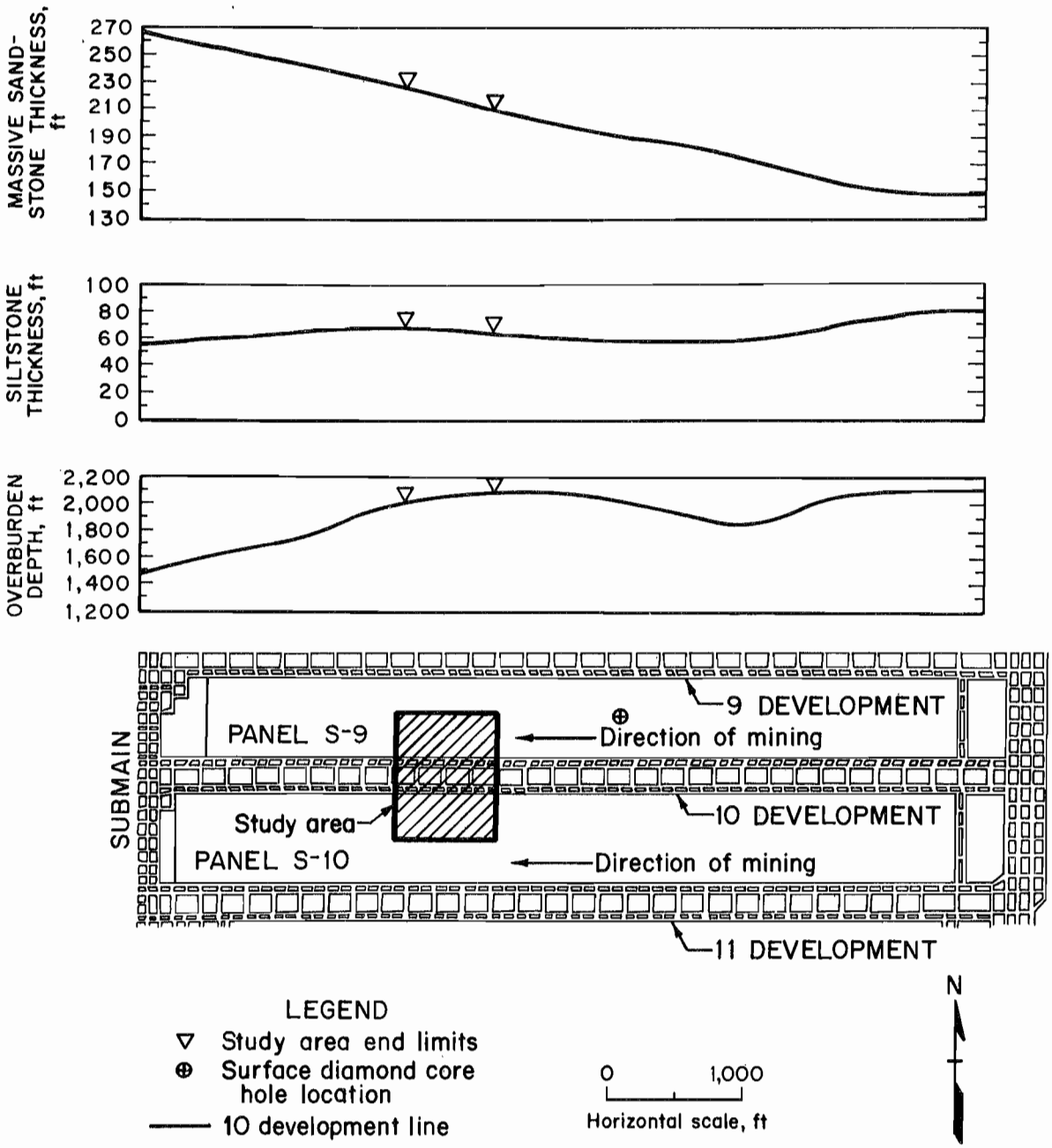

Figure 12.—Superjacent strata conditions over 10 development gate-entry system.

STUDY AREA LITHOLOGY AND PHYSICAL PROPERTIES

VERTICAL SAMPLING FROM SURFACE COREHOLE

An NX-size corehole was drilled and logged near the center of the S-9 panel, from the surface to a depth of 2,249 ft (fig. 13). The corehole intercepted the Pocahontas No. 3 Coalbed at a depth of 2,094 ft and continued to 150 ft below the coalbed (fig. 14). A registered geologist used standard surface core logging procedure (fig. 15) to generate a detailed lithographic log of the strata above and below the Pocahontas No. 3 Coalbed (figs. 16-20). Upon completion of the geologic logging, three geophysical logging runs were also made by a registered geophysicist.

The quality and strength of several rock units above and below the Pocahontas No. 3 Coalbed were comprehensively tested for physical properties in the laboratory. Throughout the stratigraphic column, representative samples of the different rock types were selected for physical properties testing. This testing included the determination of the uniaxial compressive strength for all the samples and selected testing for Young's modulus and Poisson's ratio. Young's modulus and Poisson's ratio values were calculated at 50% of the uniaxial failure strength. Rock quality designation (RQD) values were also calculated for selected samples from the immediate roof and floor. The purpose of the rock property testing, logging, and core drilling was to enhance numerical modeling efforts.

Samples from the 10 individual rock types above and below panel S-9 were tested. The units sampled may be located in relation to the Pocahontas No. 3 Coalbed by referring to the detailed stratigraphic column (figs. 16-20). These rock types tested include crystallized crossbedded sandstone (table 1), crystallized massive sandstone (table 2), crystallized quartz pebble conglomerate (table 3), crystallized sandstone with shale streaks (table 4), crossbedded sandstone (table 5), massive sandstone (table 6), sandstone with shale streaks (table 7), sandy shale (table 8), shale with sandstone streaks

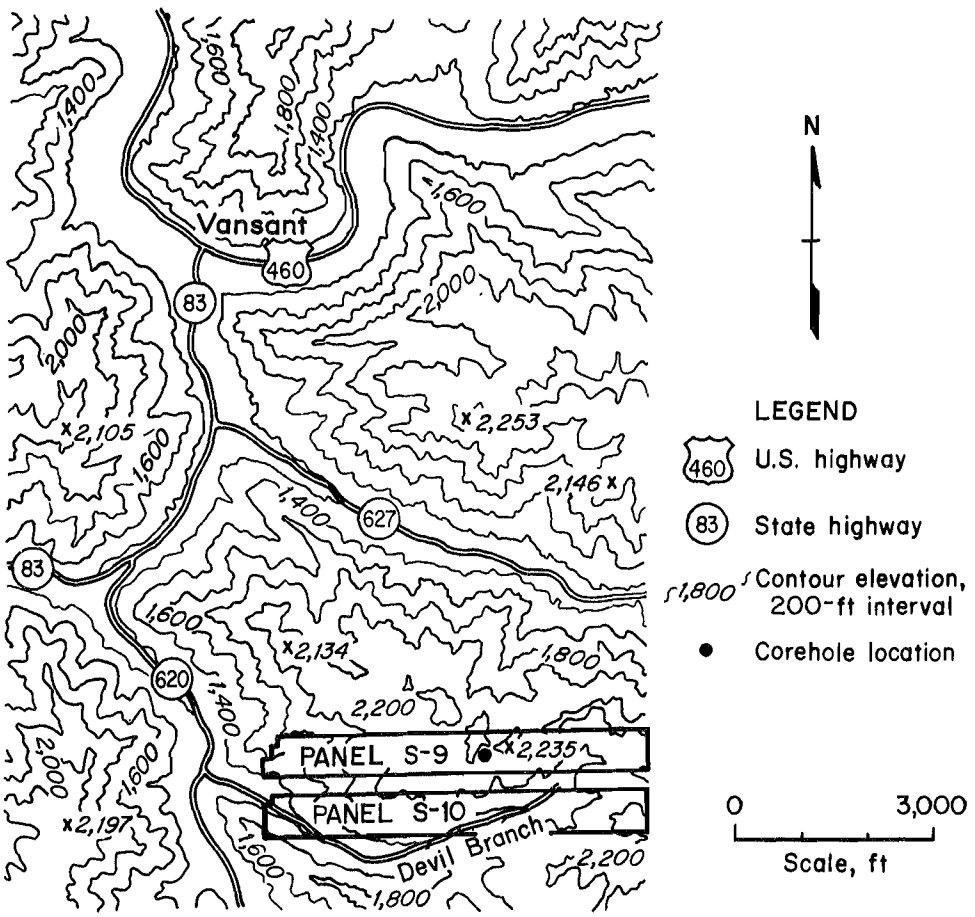

Figure 13.—Surface location of vertical corehole.

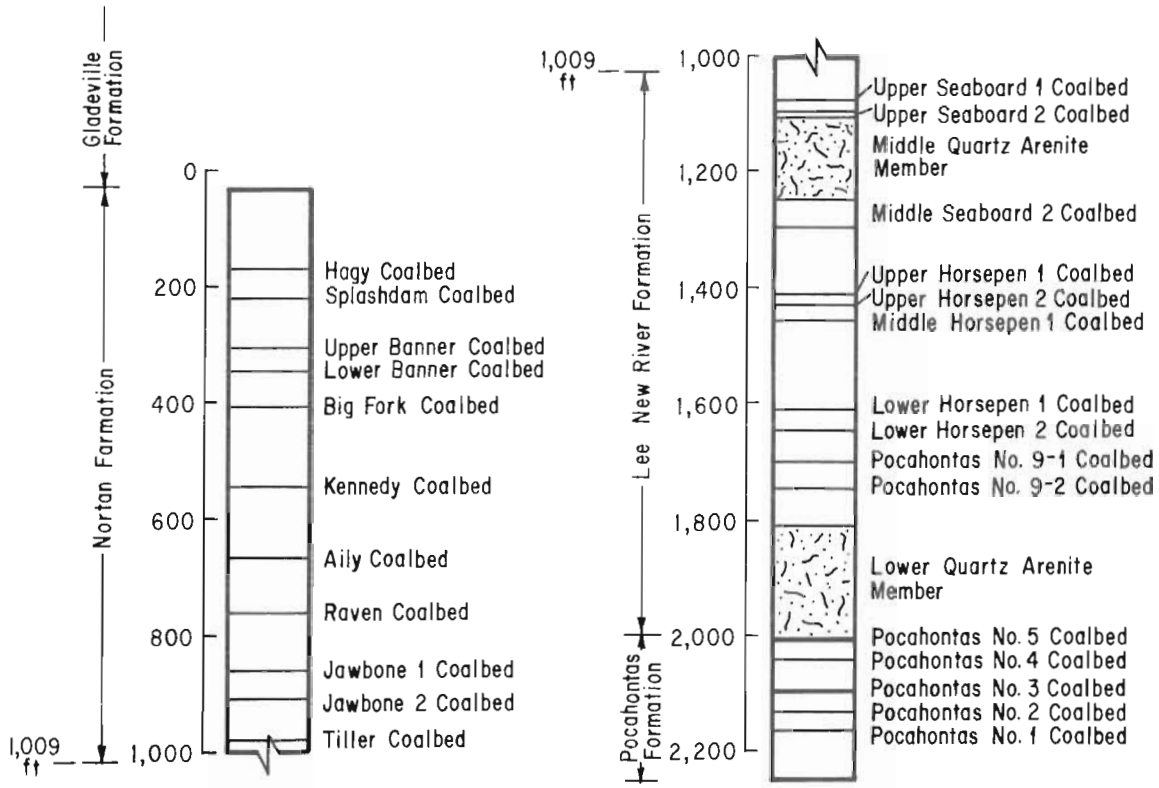

Figure 14.—Generalized stratigraphic column from vertical core logging.

Figure 15.—Surface core logging procedure.

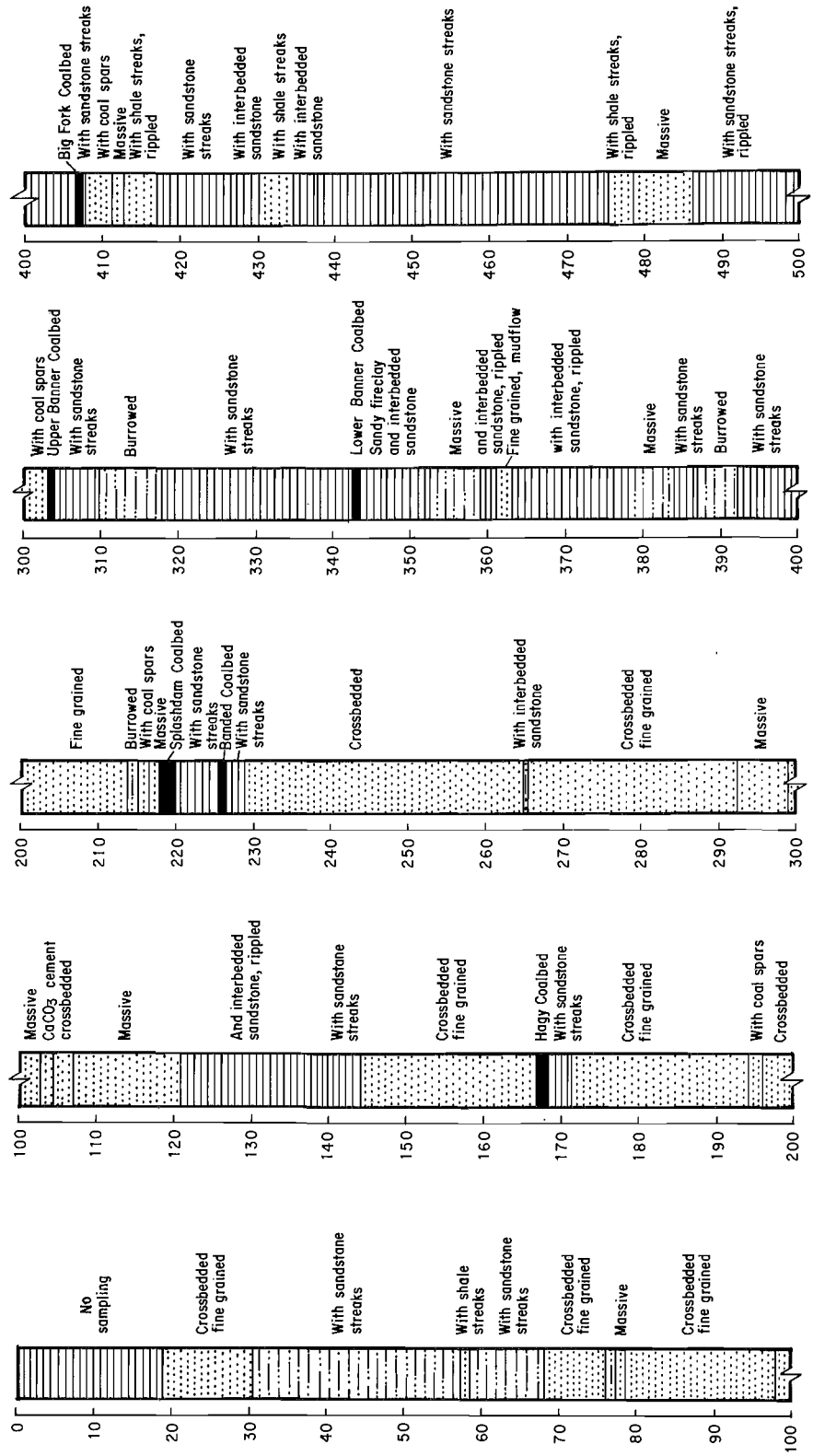

Figure 16.—Lithographic log for 0- to 500-ft depth.

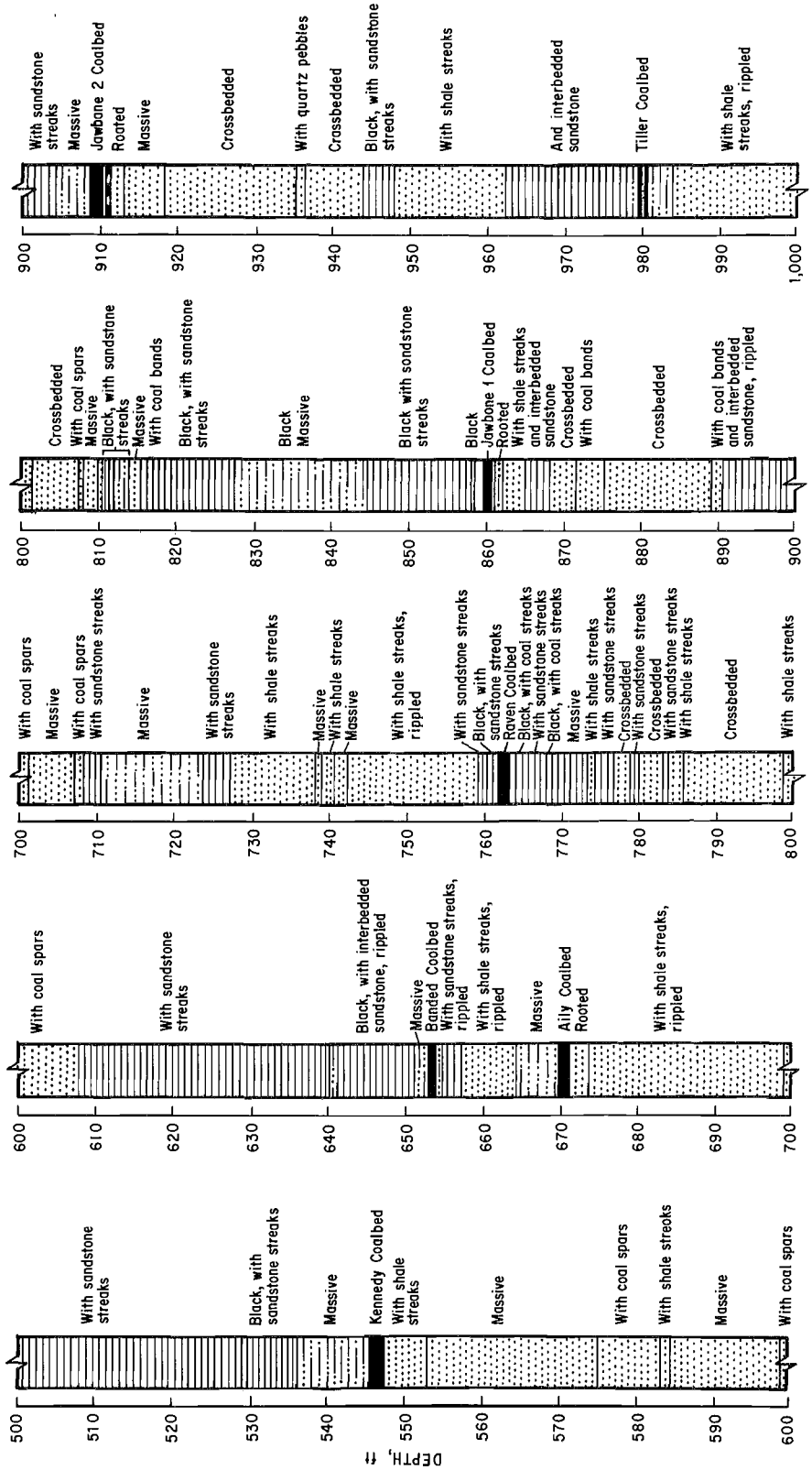

Figure 17.—Lithographic log for 500- to 1,000-ft depth.

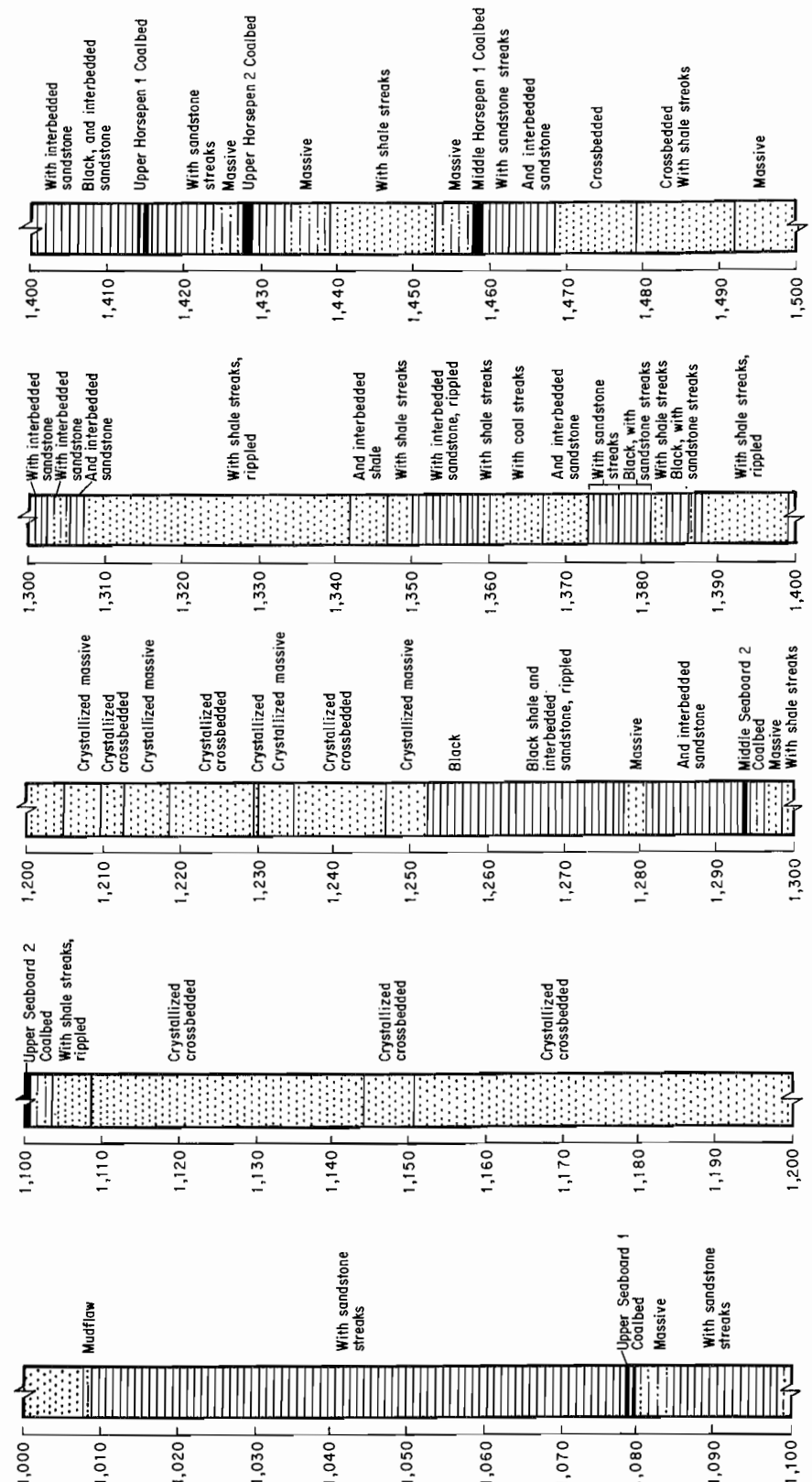

Figure 18.—Lithographic log for 1,000- to 1,500-ft depth.

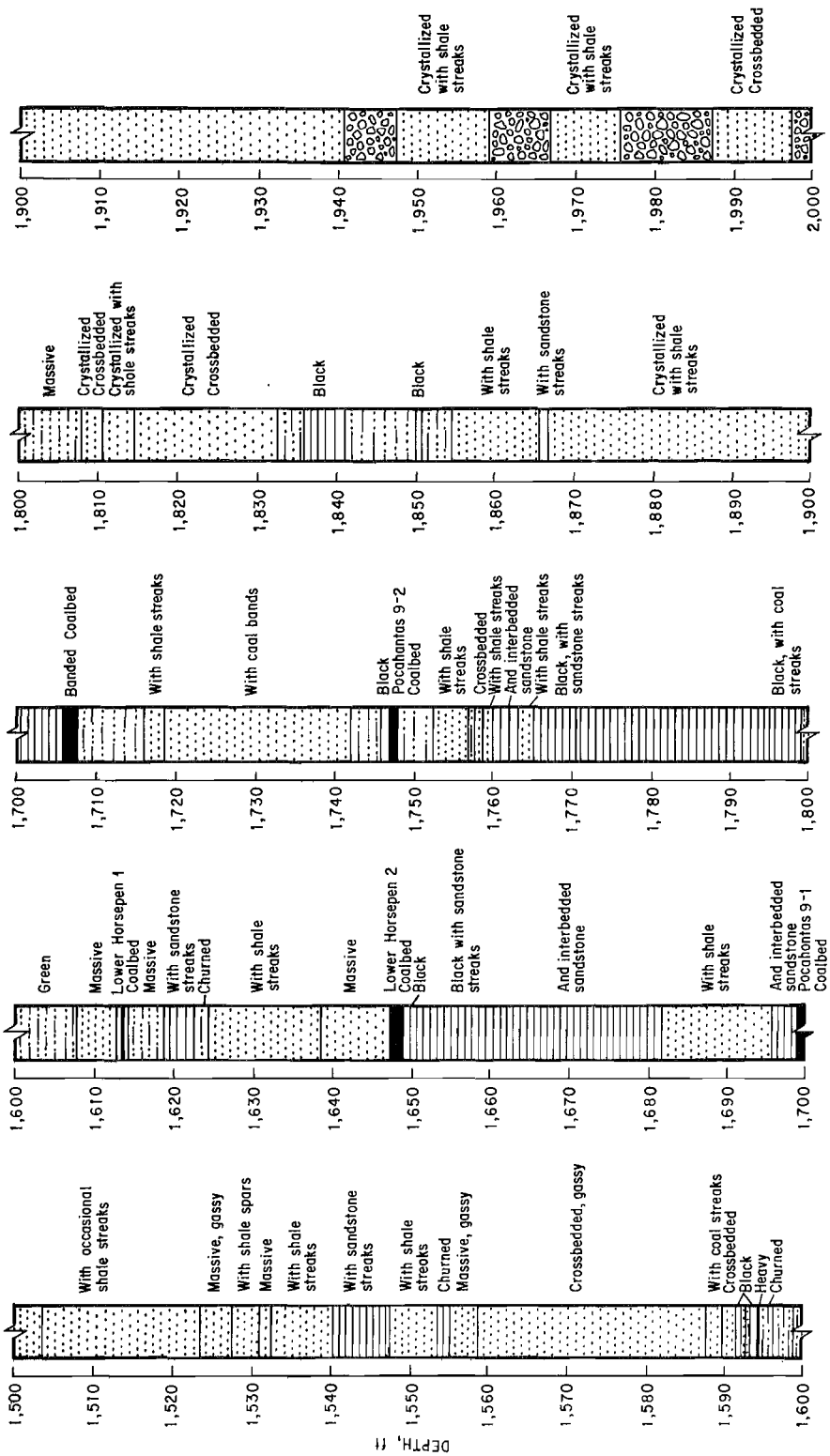

Figure 19.—Lithographic log for 1,500- to 2,000-ft depth.

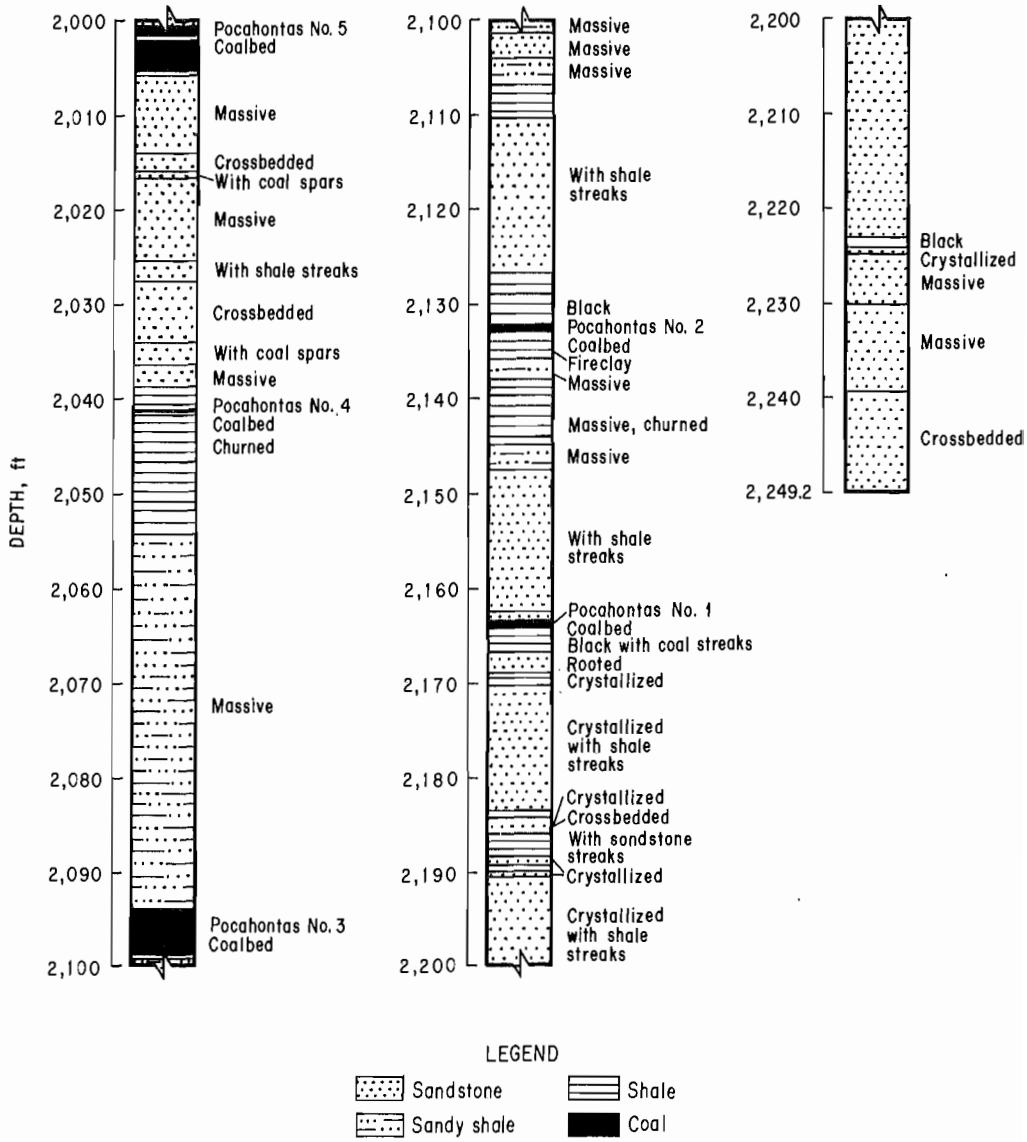

Figure 20.—Lithographic log for 2,000- to 2,249-ft depth.

Table 1.—Crystallized crossbedded sandstone from surface corehole

(Ferm's 551 mean uniaxial compressive strength = 28,590 psi)

Depth, ft	Uniaxial compressive strength, psi	Depth, ft	Uniaxial compressive strength, psi
1,111.00 to 1,111.35 . . .	24,731	1,236.30 to 1,236.36 . . .	30,966
1,117.70 to 1,118.05 . . .	24,932	1,244.60 to 1,244.96 . . .	26,722
1,120.50 to 1,120.85 . . .	25,527	1,809.50 to 1,809.85 . . .	34,408
1,133.00 to 1,133.35 . . .	22,337	1,828.55 to 1,828.90 . . .	30,689
1,137.50 to 1,137.85 . . .	28,135	1,831.40 to 1,831.75 . . .	37,641
1,151.10 to 1,151.45 . . .	26,683	1,988.50 to 1,988.85 . . .	29,345
1,167.15 to 1,167.50 . . .	26,683	1,994.00 to 1,994.35 . . .	32,494
1,167.90 to 1,168.25 . . .	25,522	2,184.00 to 2,184.35 . . .	20,804
1,178.70 to 1,179.05 . . .	28,057	2,184.50 to 2,184.85 . . .	34,191
1,190.20 to 1,190.55 . . .	33,134	2,184.85 to 2,185.20 . . .	24,199
1,198.70 to 1,199.05 . . .	28,373	2,185.20 to 2,185.55 . . .	37,990
1,213.10 to 1,213.45 . . .	21,013	2,185.60 to 2,185.95 . . .	29,783
1,227.20 to 1,227.55 . . .	30,281		

Table 2.—Crystallized massive sandstone from surface corehole

(Ferm's 554 mean uniaxial compressive strength = 32,210 psi)

Depth, ft	Uniaxial compressive strength, psi
1,143.40 to 1,143.75	35,174
1,207.10 to 1,207.45	22,639
1,217.00 to 1,217.35	29,428
1,232.00 to 1,232.35	41,608

Table 3.—Crystallized quartz pebble conglomerate from surface corehole

(Ferm's 754 mean uniaxial compressive strength = 24,660 psi)

Depth, ft	Uniaxial compressive strength, psi	RQD, %
1,959.60 to 1,959.95	35,033	100
1,966.60 to 1,966.95	24,919	100
1,978.00 to 1,978.35	15,791	100
1,986.00 to 1,986.35	22,714	100
1,998.50 to 1,998.85	24,848	100

Table 4.—Crystallized sandstone with shale streaks from surface corehole

(Ferm's 553 mean uniaxial compressive strength = 29,580 psi)

Depth, ft	Uniaxial compressive strength, psi	Young's modulus, 10^6 psi		Poisson's ratio	RQD, %
		E sec	E tan		
1,869.10 to 1,869.45	37,264	NA	NA	NA	100
1,886.20 to 1,886.55	39,190	NA	NA	NA	97.8
1,909.05 to 1,909.40	24,084	NA	NA	NA	94
1,939.00 to 1,939.35	34,378	4.571	7.644	0.078	100
1,939.35 to 1,939.70	37,361	5.050	7.620	.126	100
1,939.70 to 1,940.05	34,726	5.039	7.743	.064	100
1,955.60 to 1,955.95	40,690	NA	NA	NA	100
1,972.35 to 1,972.70	3,959	NA	NA	NA	100
2,169.95 to 2,170.30	24,194	NA	NA	NA	NAp
2,181.60 to 2,181.95	22,119	NA	NA	NA	NAp
2,191.50 to 2,191.85	25,118	NA	NA	NA	NAp
2,209.65 to 2,110.00	31,900	NA	NA	NA	NAp

NA Not available.
NAp Not applicable.

Table 5.—Crossbedded sandstone from surface corehole

(Ferm's 541 mean uniaxial compressive strength = 20,820 psi)

Depth, ft	Uniaxial compressive strength, psi	RQD, %
2,028.20 to 2,028.55	21,125	100
2,029.10 to 2,029.45	18,698	100
2,029.45 to 2,029.80	18,615	100
2,032.80 to 2,033.15	25,962	100
2,245.20 to 2,245.55	22,722	NAp
2,245.55 to 2,245.90	23,029	NAp
2,245.90 to 2,246.25	15,961	NAp
2,246.25 to 2,246.55	20,030	NAp
2,248.55 to 2,248.90	21,211	NAp

NAp Not applicable.

Table 6.—Massive sandstone from surface corehole

(Ferm's 544 mean uniaxial compressive strength = 24,170 psi)

Depth, ft	Uniaxial compressive strength, psi	Young's modulus, 10^6 psi		Poisson's ratio	RQD, %
		E sec	E tan		
2,006.00 to 2,006.35	23,735	NA	NA	NA	100
2,009.80 to 2,010.15	23,974	NA	NA	NA	100
2,012.60 to 2,012.95	22,899	NA	NA	NA	100
2,025.30 to 2,025.65	31,389	NA	NA	NA	100
2,038.00 to 2,038.35	19,880	NA	NA	NA	100
2,101.70 to 2,102.05	19,549	6.527	5.968	0.197	100
2,102.05 to 2,102.40	20,122	6.660	6.353	.212	100
2,103.85 to 2,104.20	30,735	4.580	6.041	.069	100
2,230.40 to 2,230.75	24,579	NA	NA	NA	NAp
2,239.35 to 2,239.70	24,842	NA	NA	NA	NAp

NA Not available.
NAp Not applicable.

Table 7.—Sandstone with shale streaks from surface corehole

(Ferm's 543 mean uniaxial compressive strength = 20,370 psi)

Depth, ft	Uniaxial compressive strength, psi	Young's modulus, 10^6 psi		Poisson's ratio	RQD, %
		E sec	E tan		
1,856.50 to 1,856.85	29,442	NA	NA	NA	100
1,857.00 to 1,857.35	27,842	NA	NA	NA	100
1,859.10 to 1,859.45	22,620	NA	NA	NA	100
2,026.00 to 2,026.35	10,982	NA	NA	NA	100
2,027.00 to 2,027.35	9,792	NA	NA	NA	100
2,111.90 to 2,112.25	10,192	NA	NA	NA	100
2,113.10 to 2,113.45	16,086	NA	NA	NA	100
2,114.30 to 2,114.65	29,717	5.753	6.276	0.138	100
2,114.65 to 2,115.00	18,261	5.157	4.849	.170	100
2,115.00 to 2,115.35	25,425	6.048	6.966	.136	100
2,116.60 to 2,116.95	20,110	NA	NA	NA	100
2,120.30 to 2,120.65	33,311	NA	NA	NA	100
2,148.70 to 2,149.05	17,892	NA	NA	NA	NAp
2,159.60 to 2,159.95	13,473	NA	NA	NA	NAp

NA Not available.
NAp Not applicable.

Table 8.—Sandy shale from surface corehole

(Ferm's 324 mean uniaxial compressive strength = 18,390 psi)

Depth, ft	Uniaxial compressive strength, psi	Young's modulus, 10^6 psi		Poisson's ratio	RQD, %
		E sec	E tan		
1,833.10 to 1,833.45	22,551	NA	NA	NA	100
1,842.70 to 1,843.05	19,763	5.561	4.904	0.291	100
1,845.60 to 1,845.95	21,058	4.140	6.195	.183	100
1,846.60 to 1,846.95	22,227	6.300	6.078	.230	100
1,800.10 to 1,800.45	18,774	NA	NA	NA	NAp
1,806.80 to 1,807.15	25,831	NA	NA	NA	NAp
2,054.10 to 2,054.45	12,027	NA	NA	NA	100
2,063.20 to 2,063.55	22,974	NA	NA	NA	100
2,073.90 to 2,074.25	13,113	NA	NA	NA	100
2,078.00 to 2,078.35	8,807	5.437	4.227	.311	100
2,083.00 to 2,083.35	20,163	7.206	4.871	.410	100
2,092.70 to 2,093.05	12,185	NA	NA	NA	100
2,100.40 to 2,100.75	6,365	NA	NA	NA	NAp
2,136.20 to 2,136.55	6,693	NA	NA	NA	NAp
2,136.90 to 2,137.25	27,545	NA	NA	NA	NAp
2,137.30 to 2,137.65	24,115	NA	NA	NA	NAp
2,137.65 to 2,138.00	28,447	NA	NA	NA	NAp

NA Not available.
NAp Not applicable.

(table 9), and dark-gray shale (table 10) (*8*). With the exception of the dark-gray shale, all of the rock types have a corresponding average uniaxial compressive strength value of between 28,590 and 17,500 psi. Thus, the strength and stiffness of the strata surrounding the Pocahontas No. 3 Coalbed are uncommonly high for coal measure rocks. Similarly, high strength and stiffness properties were reported by Iannacchione (*15*) for the strata surrounding the Pocahontas No. 4 Coalbed in bump-prone areas.

HORIZONTAL SAMPLING FROM UNDERGROUND COREHOLES

This field project was specifically designed to obtain an understanding of the load-bearing characteristics of longwall gob in the bump-prone strata of Southern Appalachia and to build upon the previously reported gate road stress and deformation data base (*3*). The goal was to continuously measure mining-induced abutment and gob consolidation pressures in the floor rock under the S-9 and S-10 longwall panels from the center of the 10 development gate road. Three-inch-diameter BPF's were specially designed for this purpose. Also, 2-in-diameter BPF's were located in the abutment pillar and 3-in-diameter BPF's were located below the center abutment pillar. A comparison of the coalbed-to-floor rock stress changes in and below the abutment pillar was used to evaluate the performance of the 3-in-diameter BPF's.

To facilitate the drilling of the required NX-size (3-in) floor boreholes, a 16-ft-long by 8-ft-deep sump was cut into the floor by a continuous mining machine. The 20-ft-wide sump was located in the center of the 10 development gate road, 3,800 ft from the setup rooms of the S-9 and S-10 longwall panels (fig. 21). Horizontal boreholes for the BPF's under the gate road abutment pillar were drilled with a post-mounted pneumatic drill, employing a full face, 3-in-diameter diamond wafer bit. A Diamant Boart[7] BBH 700 hydraulic core drill was used to drill the NX-size coreholes under the adjacent longwall panels. The main components are the drill itself, control panel, and power unit. The power unit is equipped with two hydraulic radial piston pumps, one for thrust and one for rotation, both powered by a single 40-hp, 440-V ac electric motor. Figure 22 shows the unit in position to drill a horizontal corehole under the S-9 longwall panel. A wireline core barrel capable of removing 10 ft of core per run was employed (fig. 23). Preliminary logging of all the horizontal cores was performed underground (fig. 24).

The trajectory of each corehole under the S-9 and S-10 longwall panels was verified by inclination and direction surveys upon the completion of logging each borehole. The elevation of the bottom of the S-9 longwall panel was surveyed, using a conventional level, when the longwall face was directly above the floor BPF's. The elevation of the bottom of the S-10 longwall panel was not surveyed, but was projected from the mine-wide trend (fig. 9). All of this information is represented by figure 25.

Horizontal core from projected instrument locations was boxed and transported to the Bureau's Pittsburgh Research Center's Rock Mechanics Laboratory, where detailed logging and physical properties testing was performed. These tests included the determination of the uniaxial compressive strength, Young's modulus, and Poisson's ratio for all 15 samples, which represented the 5 rock types. Young's modulus and Poisson's ratio values were calculated at 50% of the uniaxial failure strength. RQD values were also calculated for selected samples. All the rock property testing was performed parallel to the horizontal bedding plane because of the core being horizontally drilled. Samples from the five individual rock types encountered below the S-9 and S-10 longwall panels were tested. The rock type in the area of the instruments can be located in relation to the Pocahontas No. 3 Coalbed by referring to figure 25. These rock types tested include dark-gray shale, gray sandstone with shale streaks, dark-gray shale with sandstone streaks, black shale, and carbonate cemented gray sandstone (table 11). These rock property values were incorporated in the calibration procedure used to reduce the hydraulic pressure readings from the 3-in-diameter BPF to estimations of the true rock stress.

[7]Reference to specific products does not imply endorsement by the U.S. Bureau of Mines.

Table 9.—Shale with sandstone streaks from surface corehole

(Ferm's 323 mean uniaxial compressive strength = 17,500 psi)

Depth, ft	Uniaxial compressive strength, psi	RQD, %
1,865.90 to 1,866.25	18,695	100
1,866.30 to 1,866.65	16,299	100

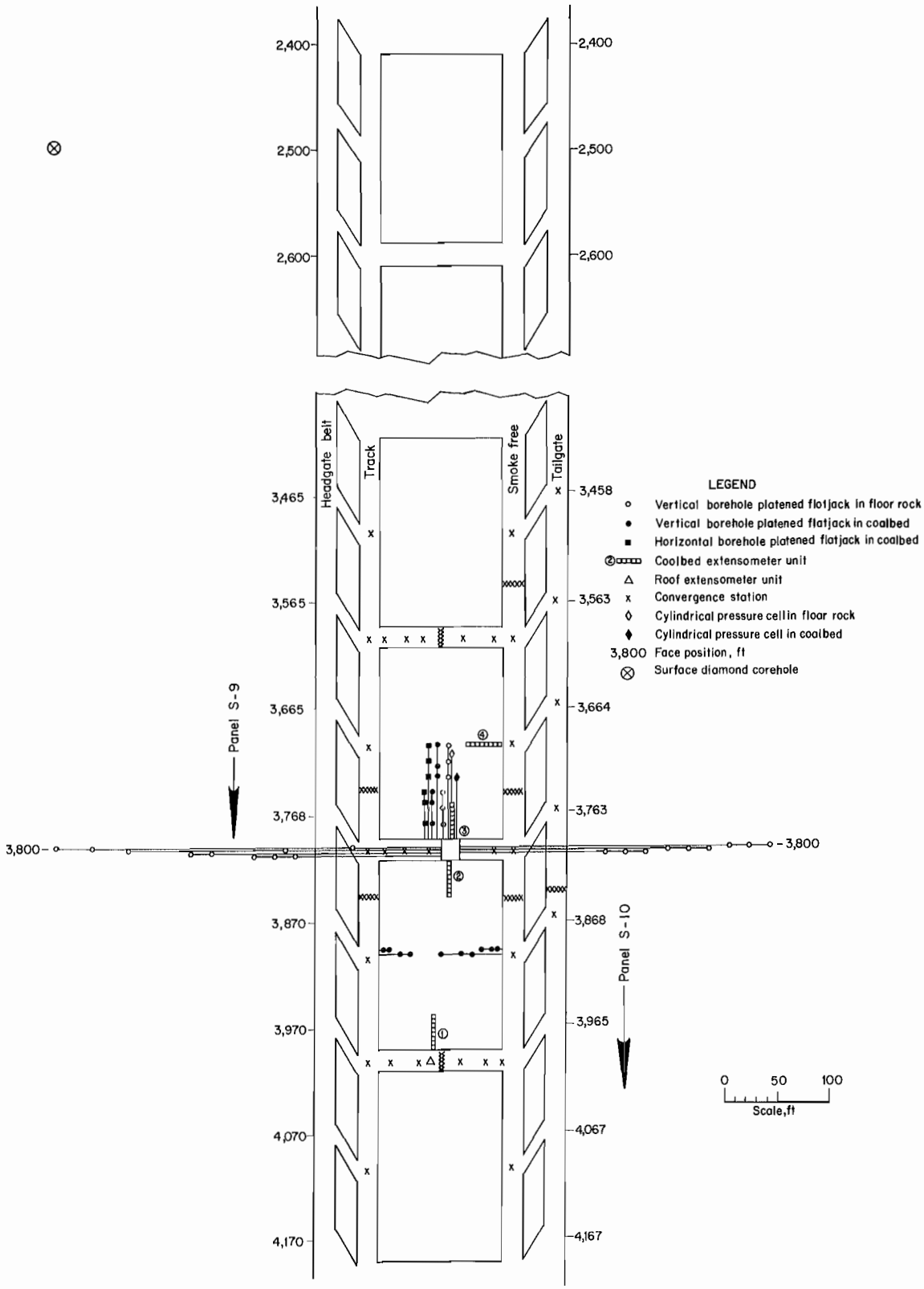

Figure 21.—Underground study area.

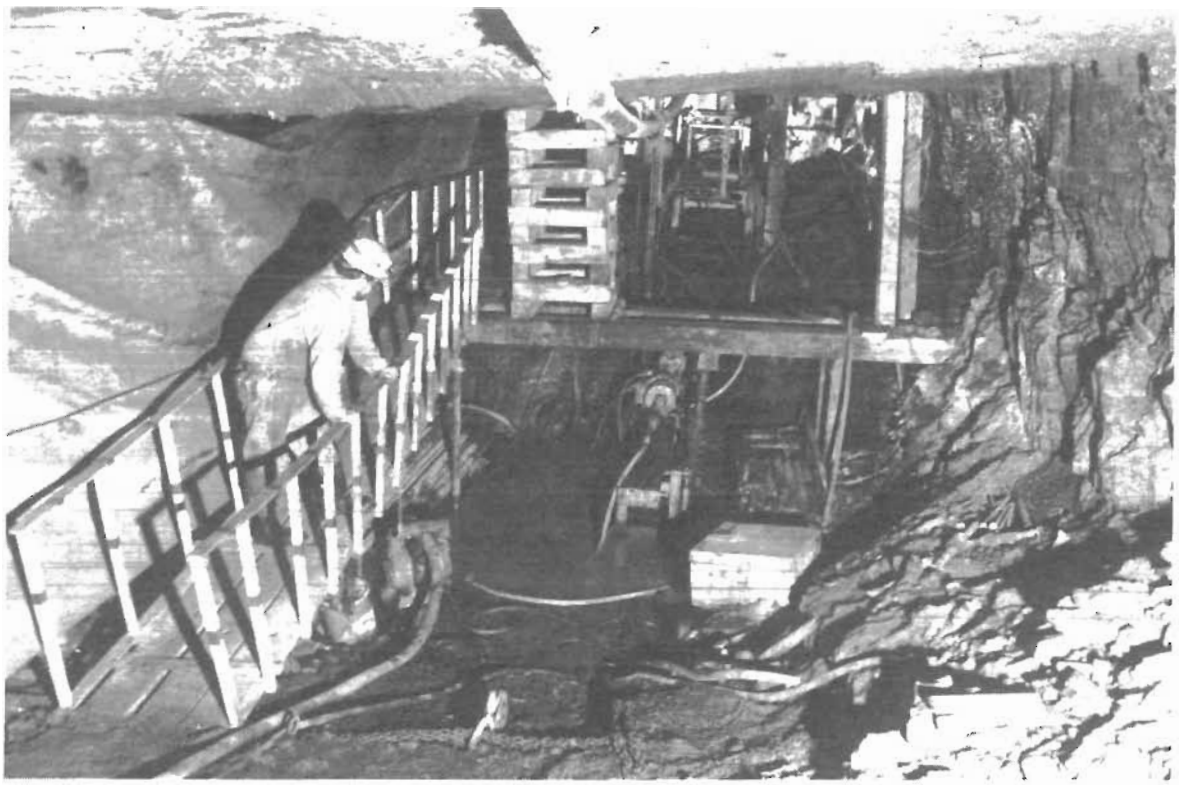

Figure 22.—Horizontal drilling technique.

Figure 23.—Horizontal core barrel retrieval.

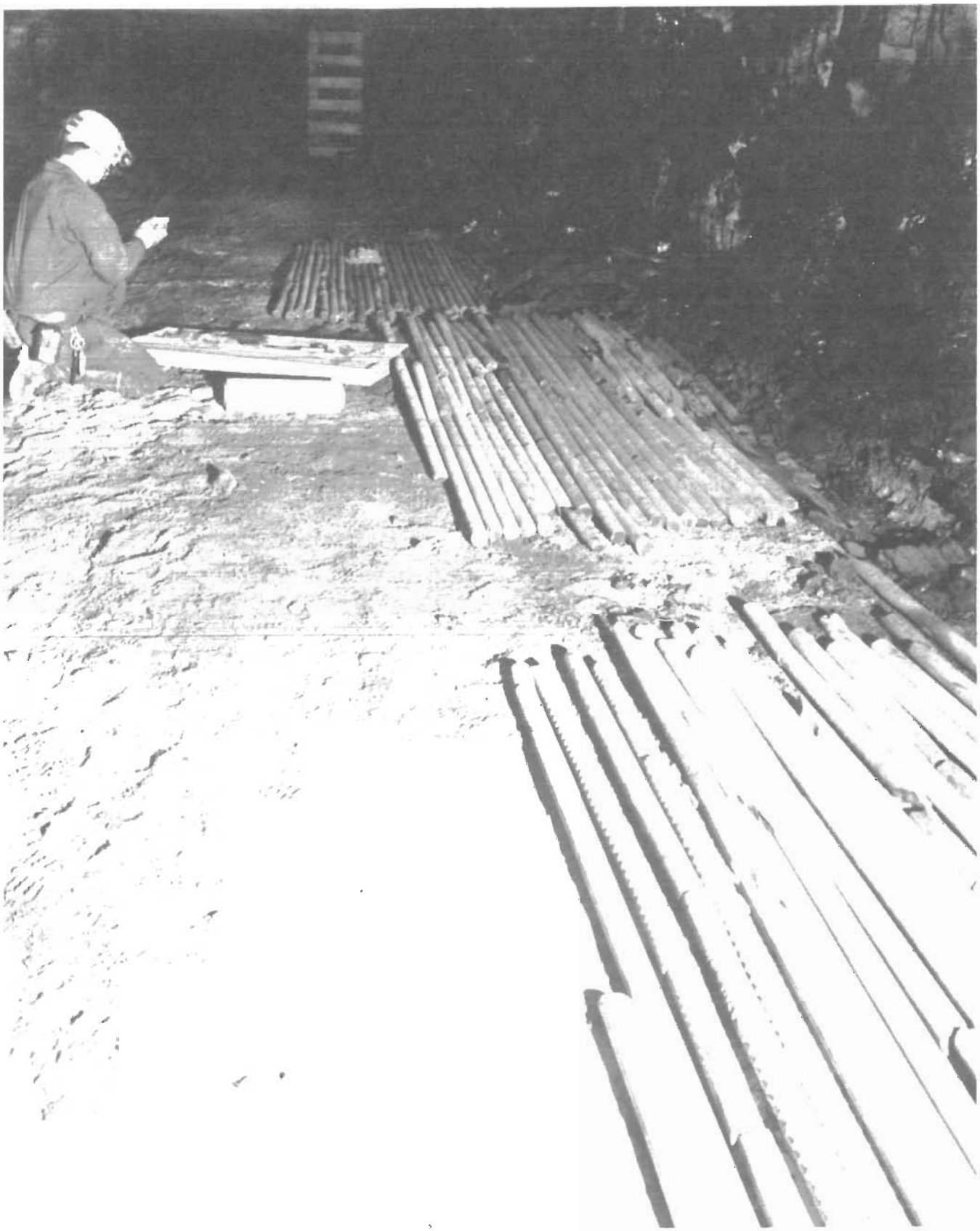

Figure 24.—Underground core logging procedure.

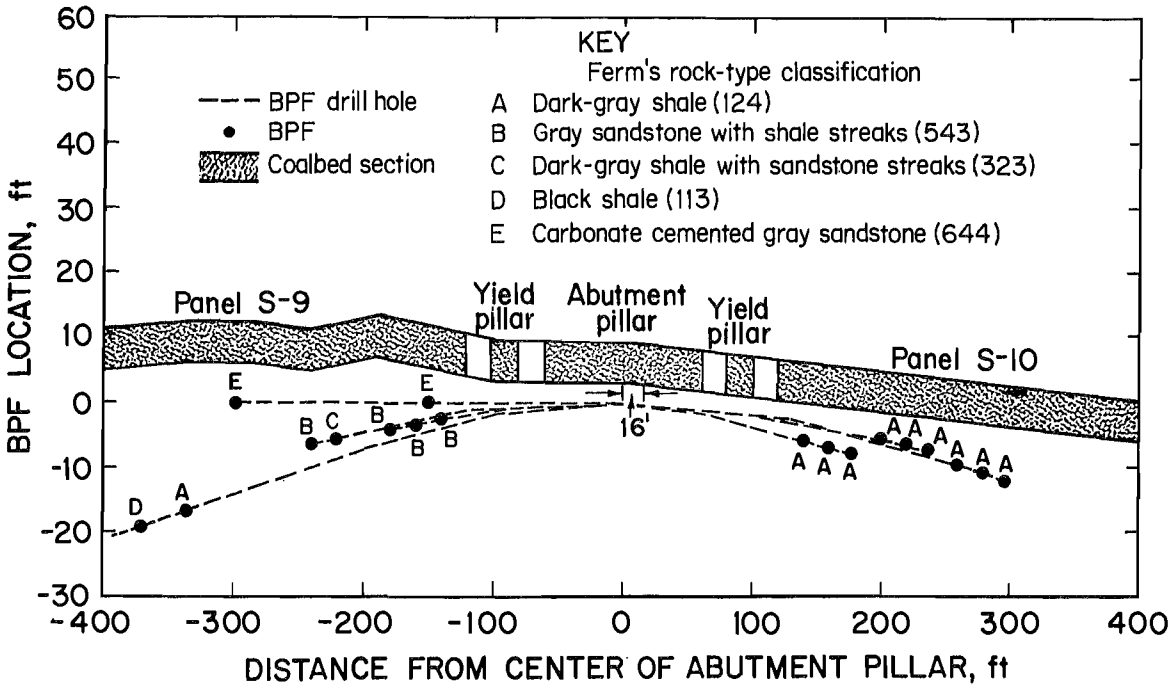

Figure 25.—Horizontal borehole deviation, BPF locations, and associated lithology.

Table 10.—Dark-gray shale from surface corehole

(Ferm's 124 mean uniaxial compressive strength = 7,650 psi)

Depth, ft	Uniaxial compressive strength, psi	RQD, %
2,048.00 to 2,048.35	6,514	100
2,138.20 to 2,138.55	8,775	NAp

NAp Not applicable.

Table 11.—Rock property test data of floor rock below panels S-9 and S-10

Panel	Horizontal borehole depth, ft	Uniaxial compressive strength, psi	Young's modulus, 10^6 psi		Poisson's ratio
			E sec	E tan	
		ROCK TYPE A[1]			
S-9	335	6,824	7.364	5.190	0.226
	335	10,839	8.587	6.830	.239
S-10	220	12,524	7.737	6.240	.343
	220	9,575	7.950	6.651	.283
	220	13,800	7.385	6.566	.336
		ROCK TYPE B[2]			
S-9	240	13,623	8.257	7.242	0.146
	240	14,410	8.571	8.201	.098
	240	15,186	8.652	7.897	.311
		ROCK TYPE C[3]			
S-9	220	5,988	6.050	6.017	0.159
	220	3,263	5.162	7.433	.170
	220	6,346	5.459	6.480	.137
		ROCK TYPE D[4]			
S-9	370	1,606	5.681	9.850	0.801
		ROCK TYPE E[5]			
S-9	300	33,410	10.277	9.909	0.230
	300	33,726	10.726	9.688	.214
	300	30,012	10.564	9.909	.220

[1]Dark-gray shale; Ferm's 124 mean uniaxial strength = 10,710 psi.
[2]Gray sandstone with shale streaks; Ferm's 543 mean uniaxial strength = 14,410 psi; RQD = 100%.
[3]Dark-gray shale with sandstone streaks; Ferm's 323 mean uniaxial strength = 5,200 psi; RQD = 100%.
[4]Black shale; Ferm's 113.
[5]Carbonate cemented gray sandstone; Ferm's 644 mean uniaxial strength = 32,380 psi; RQD = 100%.

INSTRUMENTATION LAYOUT

The state-of-the-art instrumentation array consisted of twenty-two 2-in-diameter stainless steel BPF's for indicating changes in coalbed pillar stress, eighteen 3-in-diameter stainless steel BPF's for indicating floor rock pressure changes, 4 coal extensometers for measuring pillar dilation, 77 convergence stations for measuring roof-to-floor closure, and a differential roof-sag indicator for monitoring bedding separations in the immediate roof. The instrument configurations in the 10 development gate-entry system are shown in figure 21. Campoli and Heasley (*4*) introduced this instrumentation scheme and portions of the data collected. Each of the instrumentation schemes and their results are discussed separately.

The Conspec 190 mine-wide-monitoring data acquisition system was used to remotely monitor all the rock and coal BPF's and selected convergence stations within the 10 development instrument array. The BPF's were all equipped with pressure transducers, which ranged from 0 to 30,000 psi for the 2-in-diameter coal units and 0 to 10,000 psi for the 3-in-diameter rock units (fig. 26). The pressure transducer chosen was a strain gage-type device manufactured by T-Hydronics. The transmitter is excited by a nominal 12-V dc supply and provides a 0- to 5-V dc output signal; the output voltage is proportional to the pressure. The convergence sensor is a rotary-type potentiometer (fig. 27). Several manufacturers make such

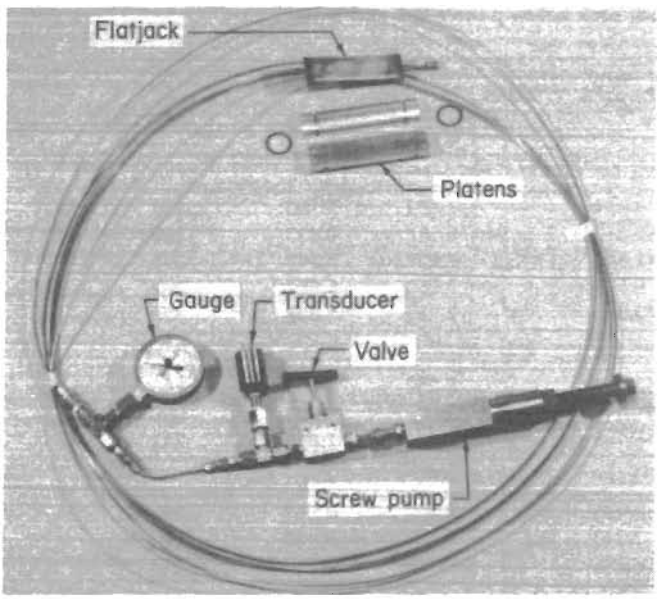

Figure 26.—BPF configuration.

devices, which provides a 0- to 500-ohm output resistance, depending upon the extension of a wire. A number of extension ranges are also available, from 2 to 2,000 in. Any convenient excitation and output voltage may be used with these devices.

Data were stored on the surface in a personal computer with Conspec software installed on the hard drive. An uninterruptable 110-V ac power supply was located on the surface and provided for data storage in the event of surface power outages. Two telephone modems, one on the surface and one at the beginning of the 10 development gate road, at the fresh-air underground outstation, allowed for communication over a four-conductor shielded signal line. This trunk line is connected to the underground modem, which provided 24 V dc to the electrical cable that is run from the trunk extender to the power barrier. The voltage is then stepped down to 15 V dc at the power barrier (fig. 28). Another trunk line is then run from the outstation power barrier in fresh air to the monitoring sites in return air (fig. 29). Attached to the trunk line at each instrument site is an accessor box with card (fig. 30). These cards take the analog signal from either a BPF

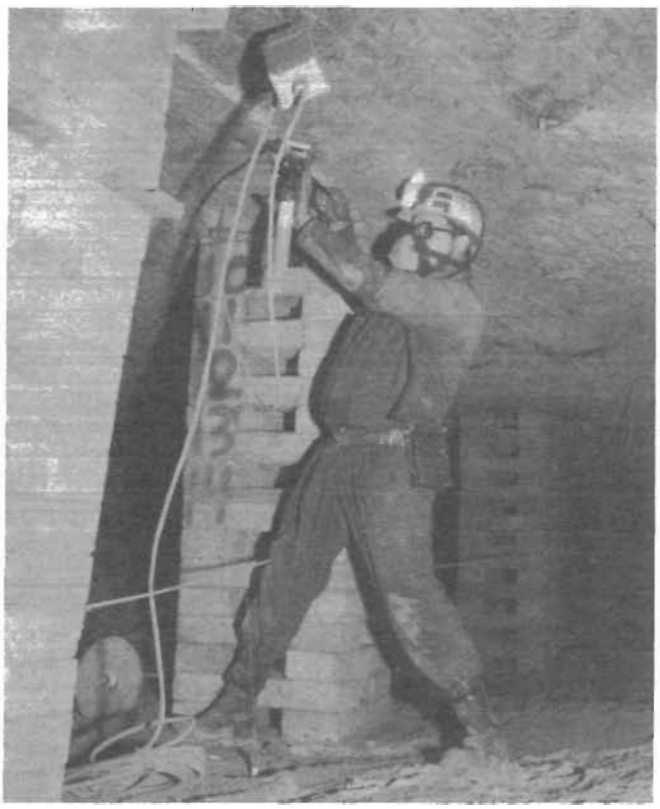

Figure 27.—Rotary-type potentiometer, remote reading, and roof-to-floor convergence sensor assembly.

transducer or a rotary potentiometer of a convergence station and digitize it for transmission to the surface.

The Conspec software samples each instrument at 5-s intervals. A command is sent over the modem line asking for a reading on a specific address. Each accessor has its own address and only that accessor will respond by obtaining its current reading. The individual assessors will then send its current reading by way of the trunk line that goes to the underground outstation for transmission to the surface computer. This surface computer will both display the current reading and store it in a historical trend file if the reading has changed by more than 1% since the last stored value. The trend files can be plotted at the operator's discretion.

Figure 28.—Data acquisition system's fresh-air outstation equipment.

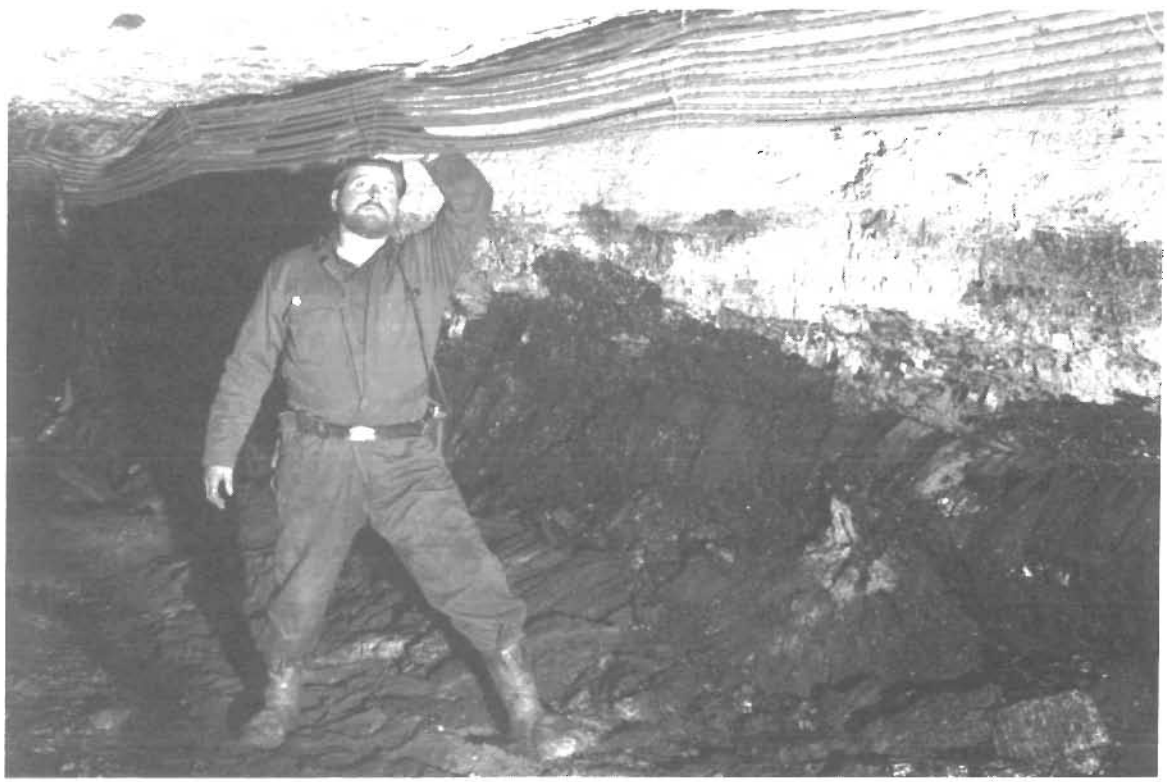

Figure 29.—Permissible data acquisition system's cables from instrument array to fresh-air outstation.

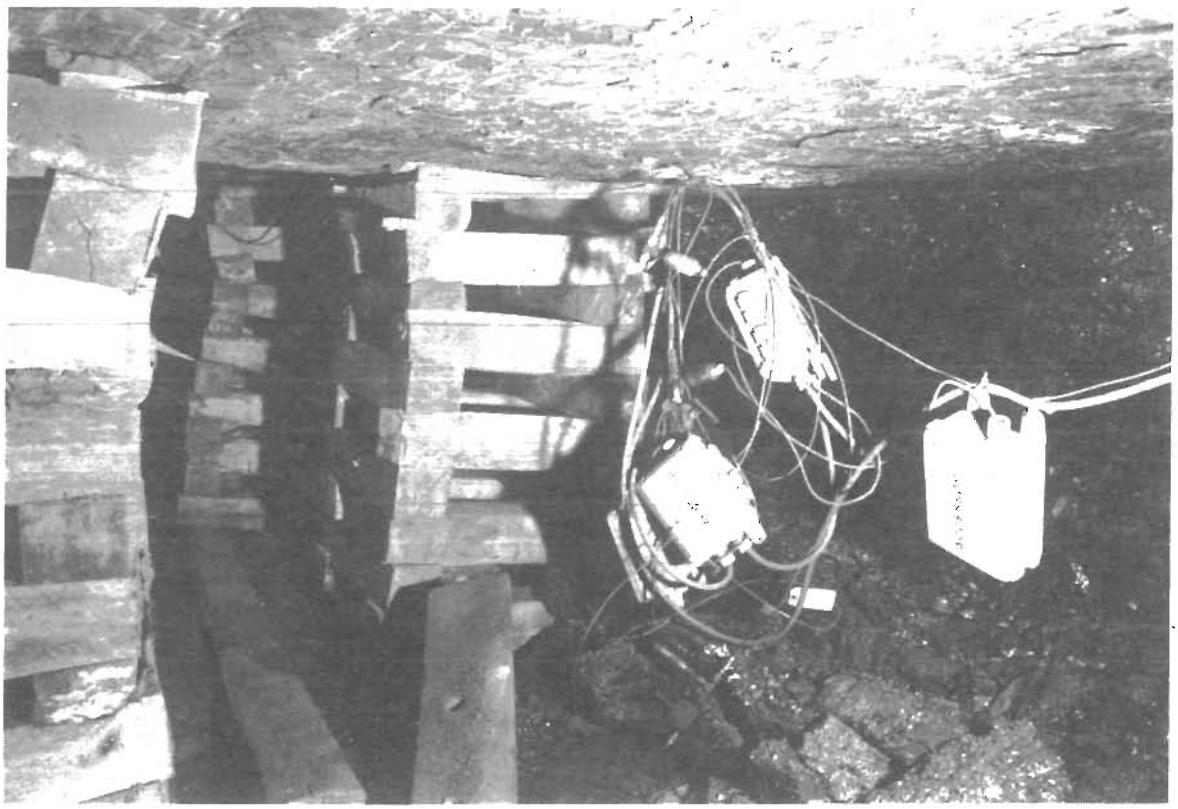

Figure 30.—Permissible data acquisition system's accessor boxes within instrument array.

GATE-ENTRY SYSTEM PERFORMANCE

ABUTMENT PILLAR COALBED STRESS CHANGE

The Bureau designed, manufactured, tested, and calibrated the BPF's used in this study. The BPF is simple in design and rugged in construction (fig. 26). The installation of the BPF is simple and straightforward. Setting rods, which allow horizontal and rotational control, enabled the BPF units used in this study to be placed in either 2-in-diameter boreholes that were drilled at mid-seam height or 3-in-diameter boreholes that were drilled in the floor rock. An electrical mercury-leveling switch was employed to ensure that the 3-in BPF's were oriented to measure the vertical stress change. The conversion of the hydraulic pressure change in the 2-in-diameter coal BPF to an approximation of the in situ stress change is accomplished with a recently developed computer program called BPFCAL (*10*). The total stress on the coalbed is calculated by adding the in situ vertical stress and the development stress to the calibrated stress change generated by BPFCAL. Borehole nonlinearities, irregularities, and installation conditions are factors that may prevent an absolute pressure conversion; however, it is felt that the calibrated BPF data are closer to actual in situ stress change in the coalbed than the uncalibrated data. Only calibrated coal BPF data will be presented in this report and will hereafter be referred to as stress change.

Where appropriate, stress change data were subjected to a linear interpolation by face position. This enables the stress change data for all BPF's to be plotted relative to face positions. A negative, zero, and positive relative face position corresponds to when the face was approaching, adjacent to, and past the instrument lines, respectively.

The 238-ft-wide 10 development gate road consisted of 20- by 80-ft yield pillars on either side of 120- by 180-ft abutment pillars. Previously reported coalbed stress change data revealed that the yield pillars in both designs experienced maximum stress and failed during the headgate pass (*3*). These walls of fractured coal, formed by the tail yield pillars, effectively shield workers from coal thrown in the event that the 120-ft-wide center tailgate abutment pillars bump during the subsequent tailgate pass. The north-south axis profile of abutment pillar stress will be used to demonstrate the gate road pillar system reaction during the mining of panels S-9 and S-10. A line of 10 BPF's located across the width of an abutment pillar

was installed at 3,900 ft from the setup rooms of the S-9 and S-10 panels (fig. 21). Data from an 11th BPF located in the geometric center of the inby abutment pillar, 3,700 ft from the start of the S-9 and S-10 panels, are also included in this analysis. The data from the two BPF's located at the geometric center of their respective abutment pillars were averaged and are shown at the 60-ft distance from the S-9 side of the center abutment pillar (fig. 31).

Minimal stress change was induced in the instrumented abutment pillar until the mining of panel S-9 reached the 600-ft face position (fig. 31*A*). At least a 5-ft yield zone was generated in the panel S-9 side of the abutment pillar when the mining of panel S-9 was between 0 and 100 ft past the instrument array. This is indicated by the drop in coalbed stress change in the BPF positioned 5 ft into the pillar (fig. 31*A*). This type of behavior is assumed to indicate the yielding of the section of the coalbed containing the BPF. Mining at the 100-ft position saw a peak stress change of near 6,000 psi on the panel S-9 side of the abutment pillar (fig. 31*A*). The yield zone in the abutment pillar enlarged to 10 ft into the panel S-9 side after the 100-ft face position, reducing the width of the confined bearing area from 120 to 110 ft. Between the 100- and 600-ft face positions of panel S-9, the peak edge stress change location shifted inward on the panel S-9 side of the abutment pillar, while stress in the pillar core and the panel S-10 side of the abutment pillar increased in value (fig. 31*B*). A 5-ft yield zone was generated in the panel S-10 side of the abutment pillar when the mining of panel S-9 moved from the 300- to the 600-ft position. At the 1,700-ft face position, a 10-ft-wide yield zone began to develop on the panel S-10 side of the center abutment pillar (fig. 31*B*).

After the 300-ft panel S-10 face position, failure of the abutment pillar's panel S-10 side occurred when the BPF located 100 ft from the panel S-9 side began to fail (fig. 32). The geometric center of the abutment pillar reaches maximum stress of 12,500 psi just prior to complete pillar failure at the 100-ft panel S-10 face position. All of the BPF's displayed negligible pressure when the final readings were taken at the 108-ft face position. The pattern and timing of abutment pillar loading and failure within the 10 development gate road are very similar to that previously reported for the 8 development gate road (*3*).

Coalbed stress change on the west-east axis of an abutment pillar was measured with vertically oriented BPF's (fig. 21). The hydraulic pressure data were reduced by BPFCAL and linearly interpolated, as were the previously discussed BPF's located on the abutment pillar north-south axis. Figure 33 graphically displays the change in coalbed stress along the west-east axis of the abutment pillar for selected face positions during the mining of panels S-9 and S-10. At the 800-ft face position of panel S-9, a peak stress change of over 10,000 psi was measured in the BPF located 15 ft from the outby edge of the

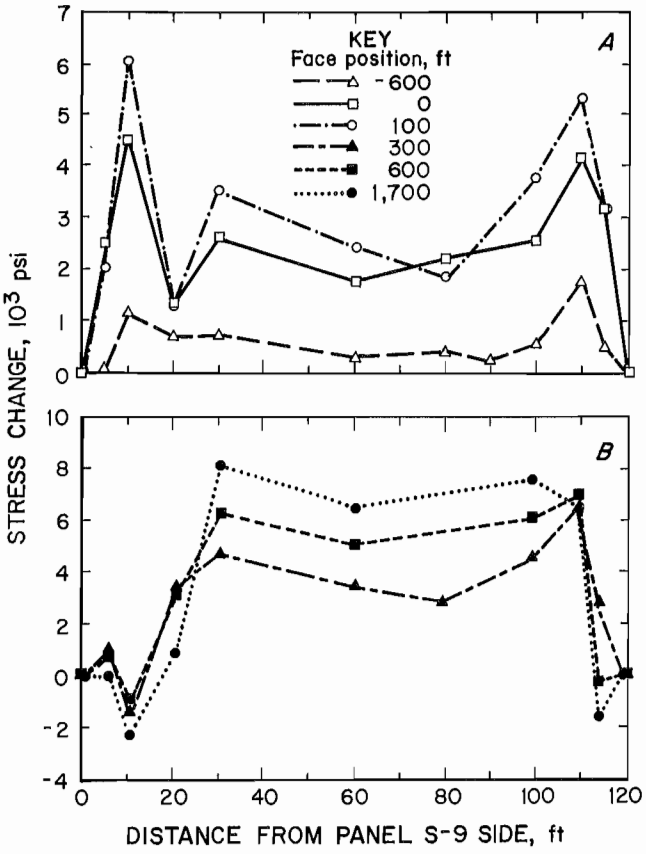

Figure 31.—Calibrated north-south profile of abutment pillar stress during mining of panel S-9. *A*, Early mining; *B*, late mining.

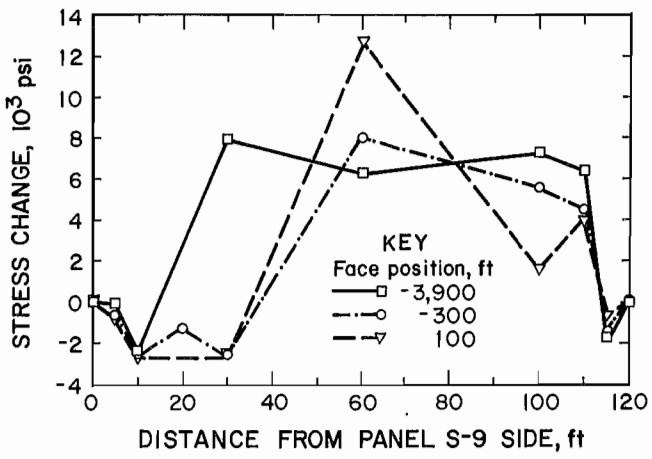

Figure 32.—Calibrated north-south profile of abutment pillar stress during mining of panel S-10.

abutment pillar (fig. 33*A*). By the -800-ft face position of panel S-10, this value was reduced to less than 7,000 psi (fig. 33*B*). Thus, the first 15 ft of the long axis of the abutment pillar was no longer part of the confined pillar core and had transferred significant load to the pillar's interior.

Analysis of figures 32 and 33*B* reveal that the effective bearing area of the 120- by 180-ft abutment pillar was reduced to a 60- by 130-ft rectangle at the 300-ft S-10 panel face position. At the 100-ft face position of panel S-10, only the geometric center of the abutment pillar continued to display a significant stress change value. Thus, it is concluded that after this point the entire pillar core was destroyed. The timing of this final destruction of the confined core is optimal since the abutment pillar is located between two gob areas and no longer of significant importance for strata control.

ABUTMENT PILLAR DILATION

Multipoint extensometers were employed to investigate the edge behavior of the highly stressed coal pillars in an attempt to further define the depth of the yielded perimeter, which confines the highly stressed core. Four coal extensometers were grouted into midseam height, horizontal drill holes at various locations, as shown in figure 21. The units were oriented to measure pillar dilation on both the long and short axes of the 120- by 180-ft abutment pillars. Each extensometer consisted of 10 anchors positioned within the first 30 ft of the abutment pillar edge. The anchors of each extensometer were positioned at 4-, 8-, 10-, 12-, 14-, 16-, 18-, 20-, 25-, and 30-ft distances from the outer edge of the abutment pillars. All units were hand read during headgate and tailgate passes (fig. 34). Thus, accessibility considerations controlled the frequency and termination of data collection.

The coal pillar dilation data were subjected to a linear interpolation by face position, just as the coalbed stress change data had been. This procedure allows for analysis at rounded distances from the face positions. Thus, the necessity for precisely matching the face positions was circumvented. These two steps allowed the coal pillar edge dilation measurements to be viewed as if the data were continuous. Again, these simplifying procedures are valid because of the consistent reaction of the coalbed, immediate roof, and immediate floor to the changing mine geometry. All of the dilation data are presented as strain (inch per inch) in a graphic format. Strain values are plotted at the midpoint of the interval between anchors. For example, an increase of 6 in. in the distance between the extensometer's head and the 4-ft-depth anchor is represented as 0.125-in/in at a 2-ft depth into the pillar.

Lateral strain recorded by extensometers 4 and 1, located in the perimeter of two adjacent abutment pillars (fig. 21), during mining of panel S-9 is graphically represented in figures 35*A* and 35*B*, respectively. A comparison of the zero-face-position stress change and coal extensometer data in the panel S-10 side of the abutment

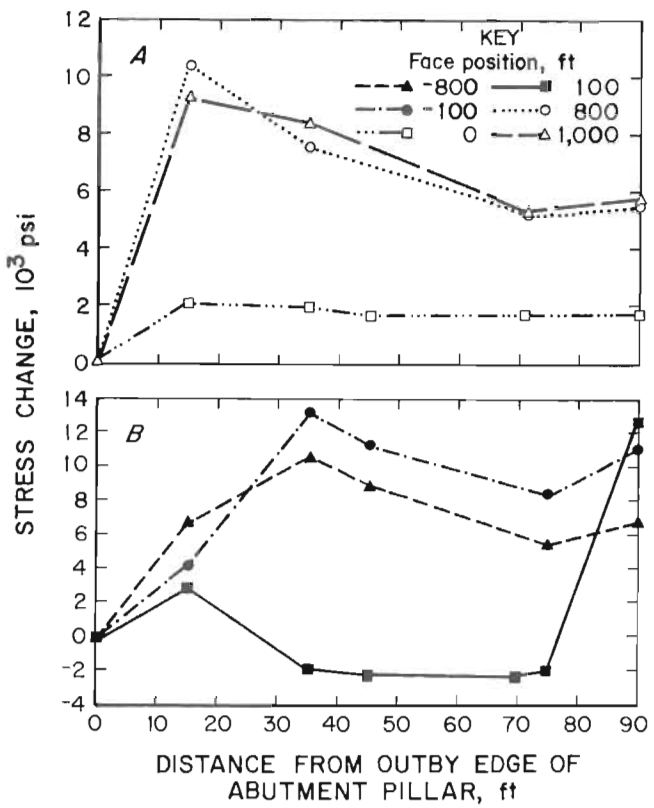

Figure 33.—Coalbed stress change on west-east axis of abutment pillar. *A*, During panel S-9 mining; *B*, during panel S-10 mining.

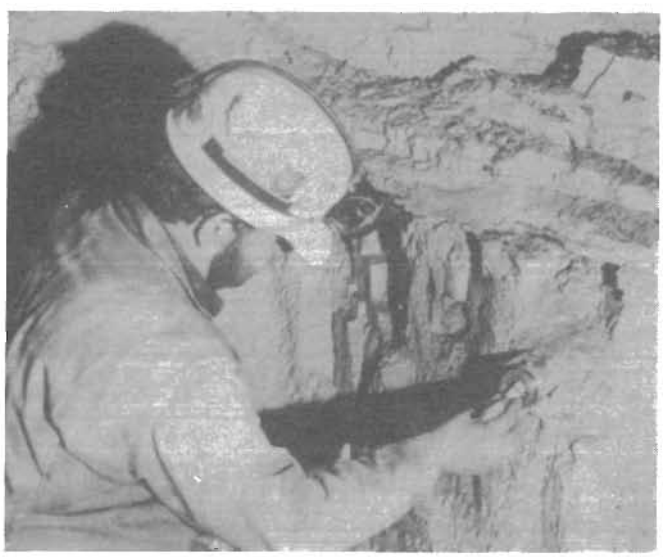

Figure 34.—Multipoint extensometer reading.

pillar of the 10 development system (figs. 31, 35*A*) both show the existence of at least a 10-ft-wide yield zone. At the 500-ft S-9 panel face position, both extensometers 1 and 4 demonstrate a 15-ft yield zone. Previously reported coal extensometer data demonstrated that highly stressed cores of Pocahontas No. 3 Coalbed pillars are confined by a minimum 15-ft-wide yielded perimeter zone around the entire pillar (*3*). Thus, the width of the yield zone in the Pocahontas No. 3 Coalbed pillars at maximum pillar load-bearing capacity is 15 ft, and that width does not significantly change when the two- dimensional size is increased. Therefore, any increase in pillar size results in a direct increase in confined core size and load-bearing capacity. Increased load subsequent to maximum load-bearing capacity increases the width of the yield zone, and the location of the peak edge stress moves toward the geometric center of the abutment pillar. Final failure occurs when the geometric center of the abutment pillar becomes part of the yielded zone.

ROOF-TO-FLOOR CONVERGENCE

In general, the convergence stations were installed in all of the nearby intersections and at the midpoints of the instrumented abutment pillars to provide an overall view of the entry closure in the study areas. Furthermore, at eight specific locations, five convergence stations were installed in a line across the entry to obtain a profile of the relative roof-to-floor closure (fig. 21). The convergence stations consisted of permanent pins installed in the roof and floor. The stations were monitored with a portable, telescoping rod, which can measure the distance between the permanent pins to within several thousandths of an inch (fig. 36). The data acquisition system was also used to remotely monitor roof-to-floor convergence. The automatic sensor employed was a rotary-type potentiometer capable of measuring up to 10 in of closure (fig. 27).

It is not possible to directly distinguish between entry closure complicated by underlying and overlying strata separation and pillar closure (vertical strain) with this methodology. The relative closures between the roof and floor are presented in this report to demonstrate the roadway response to longwall mining. Furthermore, a lack of strata separation in the immediate roof was demonstrated through a multipoint extensometer. The six-wire extensometer was located in the center of the 10 development array, 4,000 ft from the setup rooms of the S-9 and S-10 longwall panels (fig. 21). The design of and data collection from this unit was similar to the coal extensometer units (fig. 34). The mining of the S-9 and S-10 panels induced negligible roof separation over the first 40 ft of the mine roof. A total of only 0.1 in of separation was present at the -100-ft S-10 panel face position. Therefore, the researchers assume that all entry convergence is a result of main strata movement.

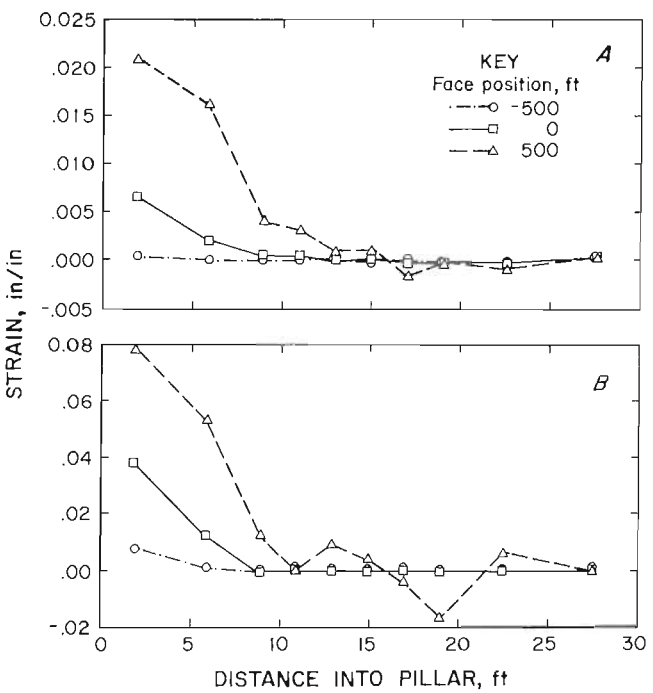

Figure 35.—Strain recorded in perimeter of abutment pillar during mining of panel S-9. *A*, Extensometer 4; *B*, extensometer 1.

Figure 36.—Roof-to-floor convergence measurement with portable telescoping rod.

Once normalized for face position, the roof-to-floor convergence data were subjected to a linear interpolation by face position, the same as the coalbed stress change and coal pillar dilation data. These two steps allowed the roof-to-floor convergence to be viewed as if all the stations were positioned along a single line from one panel edge to another. The convergence stations positioned at relatively the same distance from the S-9 panel edge within the 600-ft-long 10 development test area displayed remarkably similar behavior during the mining of the S-9 panel. The station reactions are illustrated in figure 37. This very consistent reaction of the coalbed, immediate roof, and immediate floor to the changing mine geometry is assumably due to the uniform geology over and under the instrumented test area.

The pillar stress change and roof-to-floor entry convergence data are consistent in describing the mechanism and timing of abutment pillar loading. Figure 38 graphically illustrates the magnitudes of entry convergence and stress change in and around the abutment pillars at the 500-ft S-9 panel face position (*A*) and -1,500-ft S-10 panel face position (*B*). At both face positions, an approximate convergence of 2.5 in and an approximate stress change of 6,000 psi were measured at the panel S-9 side of the confined core of the abutment pillar. The width of the effective abutment pillar confined core was reduced from 90 to approximately 40 ft as the mining of panel S-10 approached (fig. 38*B*). The parallel proportionality between convergence and stress change was obtained as a result of the uniform behavior of the roof and floor. Thus, under these geologic conditions, the mechanism and timing of abutment pillar failure may be evaluated through the measurement of either coalbed stress or roof-to-floor convergence.

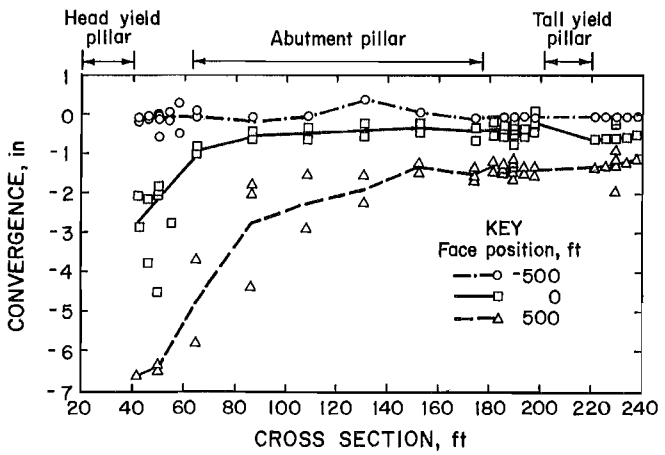

Figure 37.—Roof-to-floor convergence across 10 development gate-entry system during mining of panel S-9.

The modulus of elasticity of the Pocahontas No. 3 Coalbed was measured at 0.25, 0.55, and 0.73 million psi in three unconfined compressive strength tests on 3-in cubic samples (*3*). Two cylindrical pressure cell (CPC) tests were conducted in the Pocahontas No. 3 Coalbed within the 10 development study area. The CPC determines the in situ elastic modulus of the coal mass. The tests were performed in the abutment pillar directly inby the drilling sump, one at a depth of 45 ft and the other at a depth of 55 ft (fig. 21). The modulus results were 0.36 and 0.45 million psi, respectively. The combination of the roof-to-floor convergence of 2.5 in and stress change of 6,000 psi at abutment pillar failure yields an estimate of 0.22 million psi for the coalbed modulus of elasticity. This assumes a 3,000-psi post-gate road development abutment pillar stress and an initial coalbed height of 66 in. This realistic modulus of elasticity value lends credence to the use of convergence instrumentation to evaluate the mechanism and timing of subsequent gate road design variations.

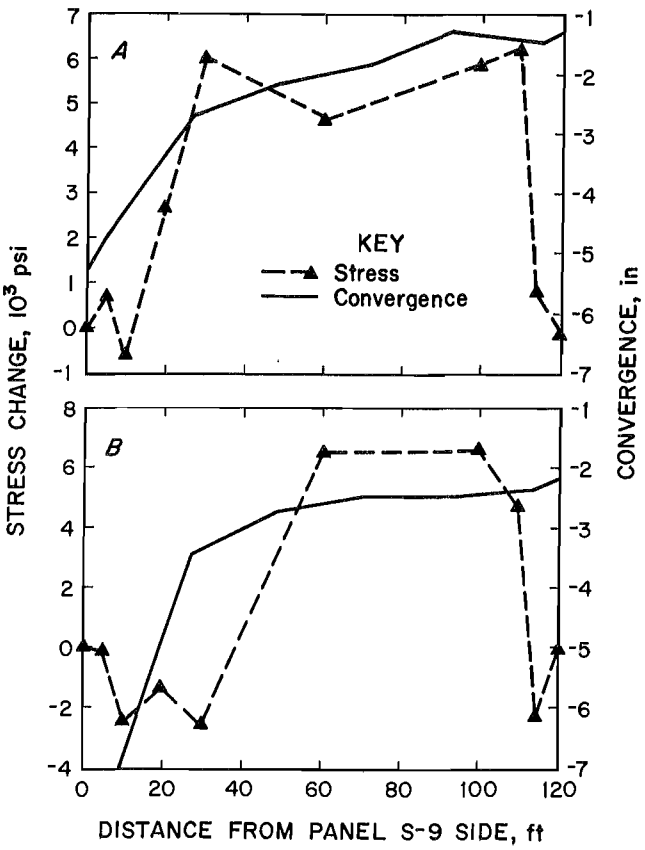

Figure 38.—Relationship between roof-to-floor convergence and abutment pillar stress change. *A*, 500-ft face position of panel S-9; *B*, -1,500-ft face position of panel S-10.

COMPARISON OF ABUTMENT PILLAR FLOOR AND COALBED STRESSES

Specially designed 3-in-diameter BPF's were installed in the floor rock directly below the coal BPF positioned on the abutment pillar's long (west-east) axis (fig. 21). The conversion of the hydraulic pressure change in the 3-in-diameter rock BPF to an approximation of actual in situ stress change was accomplished with a modified version of BPFCAL (*10*). Two CPC tests were conducted in the floor rock directly below the instrumented abutment pillar, one at a depth of 8 ft and the other at a depth of 90 ft (fig. 21). The modulus results from these two tests were 6.4 and 3.1 million psi, respectively. The rock surrounding the BPF under the abutment pillar was a dark-gray shale. The modulus of elasticity from five laboratory tests averaged 7.8 million psi for lateral samples of this dark-gray shale (table 11). Based on the CPC, laboratory values and a reduction for size effects, an input value of 2.1 million psi for elastic modulus of the rock mass was used in BPFCAL.

The 3-in-diameter BPF in the floor rock was 5 to 10 times stiffer than the 2-in-diameter BPF in the coal. The difference in the sensitivity of the two measurements can be demonstrated by the comparison of the floor and coalbed BPF hydraulic pressure output. The rock and coal BPF outputs 90 ft from the outby edge of the abutment pillar show a similar trend in their hydraulic pressure with their maximum readings occurring at approximately the same time; however, the maximum coal hydraulic pressure is 4.6 times higher than the maximum rock pressure (fig. 39).

Comparison of the coal and floor stress changes, 90, 75, and 45 ft from the west edge of the abutment pillar, demonstrates the variability in the BPF calibration due to local geologic anomalies or nonelastic behavior. However, the stress changes in the floor and coal both gradually increase with the passing of the panel S-9 face (fig. 40). This was not true for the floor stress change 15 ft from the west edge of abutment pillar. It increased dramatically after the 400-ft face position, surpassed the coal stress change after the 600-ft face position, and fell rapidly after the 650-ft face position (fig. 41). The peak spike in floor rock stress change occurs simultaneously with peak coalbed stress change, approximately 10,000 psi. Comparison of the coal and floor stress changes, 90, 75, and 45 ft from the outby edge of the abutment pillar during panel S-10

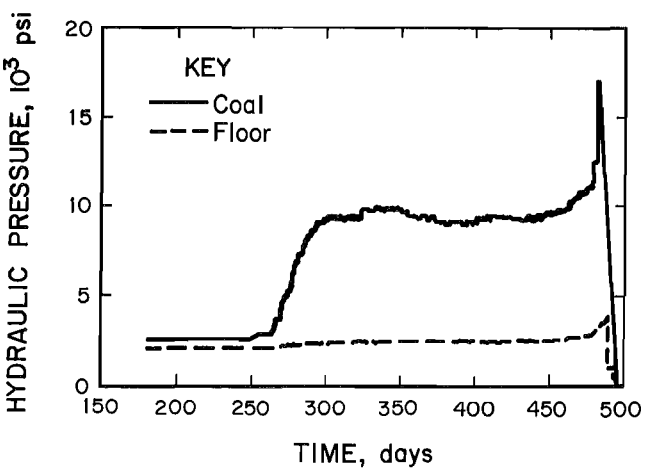

Figure 39.—Hydraulic pressure of coal and floor BPF's 90 ft from west edge of abutment pillar.

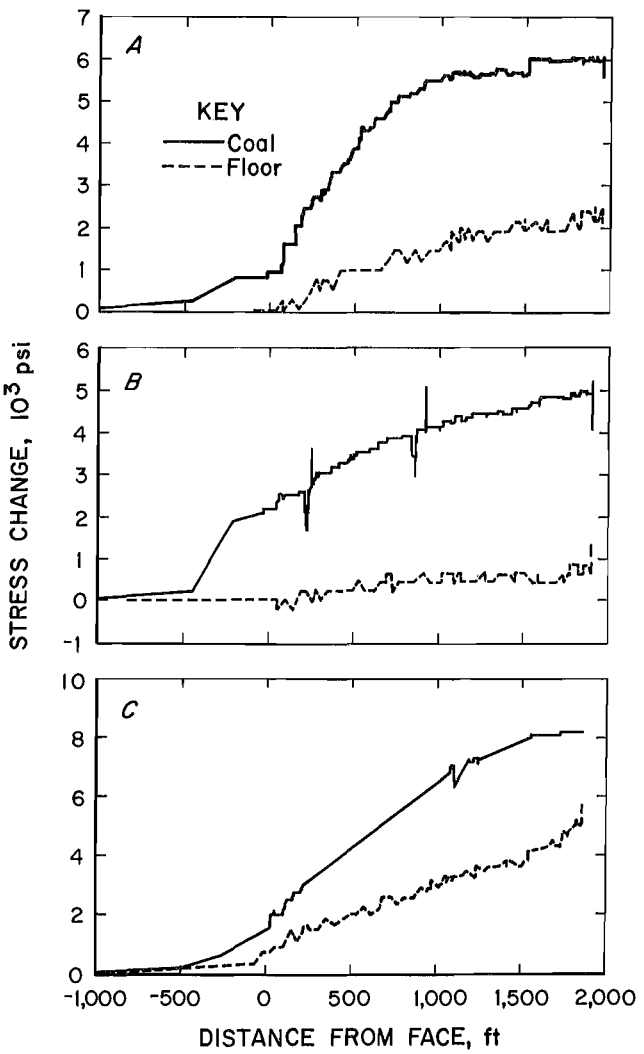

Figure 40.—Coal and floor stress changes on west-east axis of abutment pillar during panel S-9 mining. *A*, 90 ft from west edge; *B*, 75 ft from west edge; *C*, 45 ft from west edge.

mining, reveals that peak rock stress change occurred with or slightly lagging that of the coalbed peak stress change, approximately 10,000 psi (fig. 42).

Peak floor stress changes of over 18,000 psi occurred 15 and 45 ft from the west edge of the abutment pillar during the mining of panels S-9 and S-10, respectively. The peak floor stress change of approximately 10,000 psi at 75 and 90 ft from the west edge of the abutment was equivalent to the 10,000-psi peak coalbed stress change. Figures 41 and 42 show a consistent value for the peak coalbed stress change in contrast to the variable peak floor stress change. The consistent value for the peak coalbed stress change is noteworthy in contrast to the variable values for the peak floor stress change.

This behavior is attributed to a changing modulus of elasticity at the limit of rock strength. Recall that BPFCAL assumed a constant modulus of elasticity of 2.1 and 0.3 million psi for the rock and coal, respectively. It is concluded that a constant value for the modulus of elasticity may be appropriate for the coalbed, but is probably not satisfactory for the stiffer floor rock. This issue will be addressed in future research on the behavior of stiff strata at failure. However, there is consistent agreement between the timing and relative magnitude of peak floor and coalbed stress changes (fig. 42). Thus, the floor BPF data obtained from under the headgate side of the S-9 panel and the tailgate side of the S-10 panel are a valid indicator of the timing and relative magnitude of the front and side abutment loading during longwall panel mining.

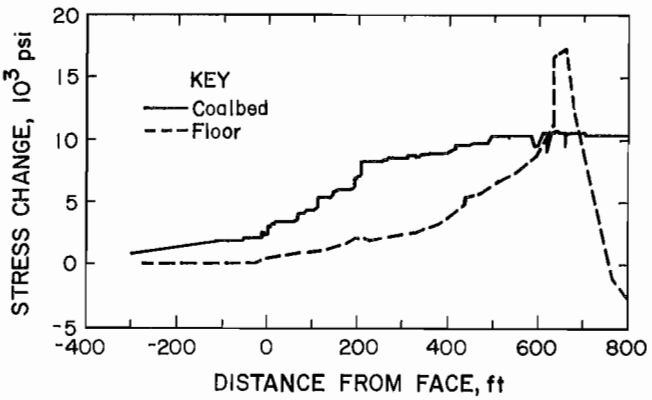

Figure 41.—Coal and floor stress changes 15 ft from west edge of abutment pillar during panel S-9 mining.

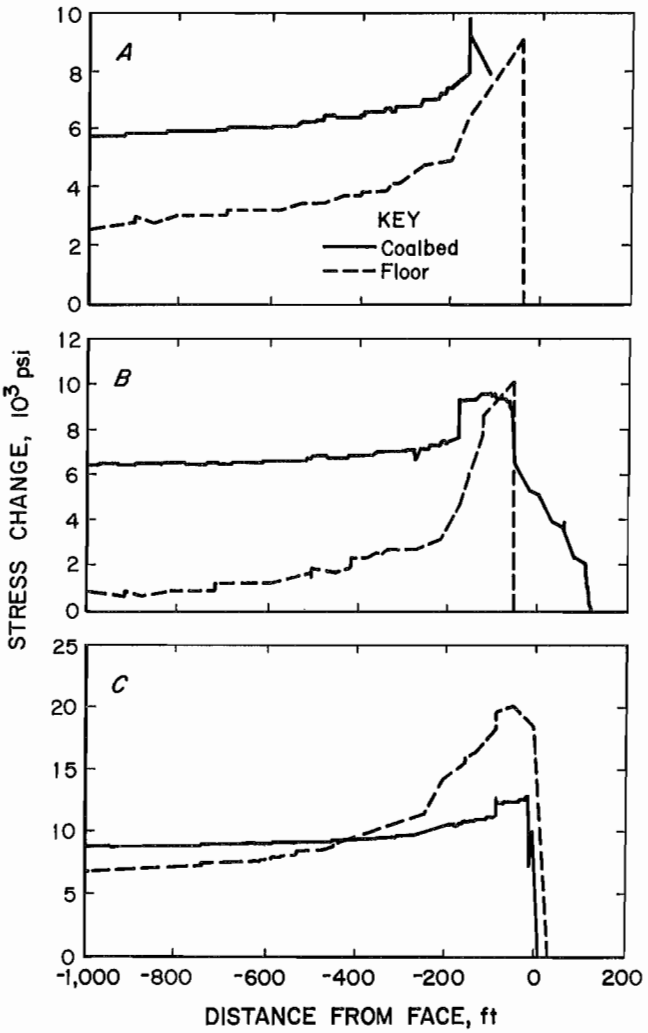

Figure 42.—Coal and floor stress changes on west-east axis of abutment pillar during panel S-10 mining. *A*, 90 ft from west edge; *B*, 75 ft from west edge; *C*, 45 ft from west edge.

LONGWALL GOB FLOOR LOADING

A total of eighteen 3-in-diameter BPF's were installed in the floor rock below panels S-9 and S-10. All these instruments were on a line approximately 3,800 ft from the setup rooms of panels S-9 and S-10 (fig. 21). Figure 25 graphically depicts the depth of each instrument below the Pocahontas No. 3 Coalbed. All nine of the BPF's below panel S-10 and the BPF 213 ft from the headgate edge of panel S-9 were located in a dark-gray shale formation, with a Ferm classification of 124 (table 11). The BPF's 18, 38, 58, and 118 ft from the headgate edge of panel S-9 were located in gray sandstone with shale streaks, with a Ferm classification of 543 (table 11). The BPF 98 ft from the headgate edge of panel S-9 was located in dark-gray shale with sandstone streaks, with a Ferm classification of 323 (table 11). The BPF 248 ft from the headgate edge of panel S-9 was located in black shale, with a Ferm classification of 113 (table 11). The BPF's 28 and 178 ft from the headgate edge of panel S-9 were located in carbonate cemented gray sandstone, with a Ferm classification of 644 (table 11).

PANEL S-9

Raw hydraulic data from the panel S-9 BPF's were taken every 2 h over the life of the study, resulting in over 2,300 data points for each of the 9 instruments during the mining of panel S-9. Prior to calibration, an analysis of gob behavior from raw pressure readings was conducted to distinguish general trends in the data. The hydraulic pressure of three representative floor BPF's, located 18, 98, and 248 ft from the headgate edge of panel S-9, are presented in figure 43. The maximum pressure values for all nine instruments occurred when the longwall face was directly above the line of instruments. The minimum pressure values for all nine instruments occurred as the longwall face mined the coal just past the line of instruments. As the face advanced, the hydraulic pressure rebounded. The instruments near the headgate edge experienced the minimum rebound, while the units nearer the center of panel S-9 experienced the maximum pressure rebound. The BPF 18 ft into the 600-ft-wide panel S-9 does not rebound at all while the 248-ft-deep BPF rebounds to a value close to the original hydraulic pressure. The 248-ft-deep BPF obtained a value nearest the original hydraulic pressure when the face was approximately 400 ft (0.2 times the overburden depth) beyond the instrument array (fig. 43).

A special effort to provide a very accurate calibration of the 3-in-diameter BPF's installed under the panel S-9 was performed. To accomplish this accurate calibration, a laboratory BPF with an identical length of tubing and an identical volume of fluid as the BPF in the field was tested in the Rock Mechanics Laboratory (fig. 44). In this test, discrete data points were duplicated for each of the BPF's by using the load frame to control the BPF hydraulic pressure. The outcome of these tests were load and displacement curves that should correspond to the load and displacement experienced by the BPF in the field. The next step in this calibration was to use these load and displacement values to back calculate the corresponding in

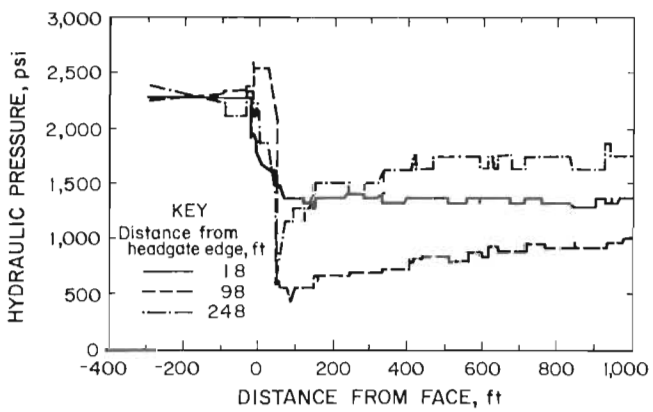

Figure 43.—Hydraulic pressure of floor BPF's under panel S-9 during panel S-9 mining.

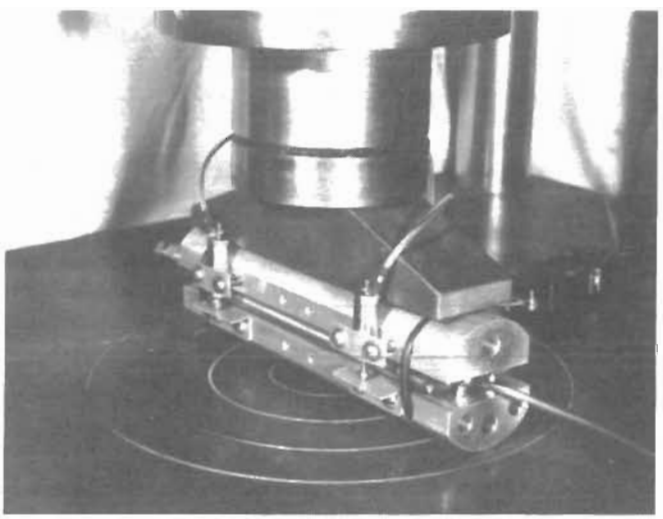

Figure 44.—BPF calibration laboratory testing.

situ stress experienced by the rock surrounding the BPF (fig. 25). The analytical equations for this back calculation were implemented in a revised version of BPFCAL.

The calibration process revealed that the BPF's were extremely sensitive to the functional in situ elastic modulus. When the laboratory values of the elastic modulus were used in BPFCAL, the calibrated results showed unreasonably high stresses. To establish a more reasonable in situ elastic modulus, an iterative process was employed to select the elastic modulus that resulted in a low-stress value of approximately zero. This model assumed that a zero-stress condition exists in the floor directly behind the face. Based on this assumption, a constant value for the elastic modulus was selected for the rock surrounding each BPF (table 12). It is likely that the modulus of elasticity of the rock surrounding the instrument changes rapidly after the assumed zero-stress condition after mining progresses. The dubious accuracy of this critical rock property probably reduced the accuracy of the calibrated stress. However, the calibrated data were useful in the analysis of the general floor stress trends. The subsequent discussion of the results of panel S-9 floor stress will be based on calibrated data only.

The front abutment peak load occurred when the face was within 20 ft of the instruments (fig. 45). The peak front abutment stress generally increases as distance from headgate edge increases. The mean and standard deviation of the peak front abutment stress are 3,893 and 1,834 psi, respectively (fig. 46). The peak stress recovery under panel S-9 generally increases as distance from headgate edge increases. No measurable stress recovery occurred in the instruments 18 and 28 ft from the headgate edge of panel S-9. BPF's nearest the center of the panel rebounded to a value closest to the original cover stress of approximately 2,310 psi (fig. 47). The peak stress recovery generally occurred at about the 400-ft face position (0.2 times the overburden thickness) (fig. 48). Panel S-9 gob floor stress was monitored during the remainder of panel S-9 mining and during panel S-10 mining without significant change of stress from that last reported in figure 45.

PANEL S-10

The rock surrounding the BPF's under panel S-10 was the same as that under the abutment pillar, dark-gray shale (figure 25 and table 11). The calibration of these nine 3-in-diameter BPF's was performed with an input value of 2.1 million psi for the elastic modulus of the rock mass. Thus, the BPFCAL data manipulation followed the procedure employed on the BPF's under the abutment pillar. The following discussion is based on the calibrated rock stress values.

The panel S-9 mining caused noticeable side abutment stress in the BPF's 38, 58, and 78 ft from the tailgate edge of panel S-10 (fig. 49*A*). However, the BPF's closer to the panel center appeared to record values only slightly greater than the original cover stress while decreasing in magnitude as their location got closer to panel center (figs. 49*B-C*). Campoli, Barton, Van Dyke, and Gauna (*3*) also measured side abutment stress near the tailgate edge of an unmined panel during mining of an adjacent panel.

Stress did not again increase in the BPF's below panel S-10 until its mining was within 100 ft of the instrument line (fig. 50). The floor stress dramatically increases to peak front abutment stress when the face is within 20 ft of the instrument line (fig. 50). The peak front abutment across the tailgate side of panel S-10 occurred at 38 and 118 ft from the tailgate edge. Discounting the malfunctioning instrument located 178 ft from the tailgate

Table 12.—Modulus of elasticity calculation iterations used in panel S-9 floor stress calibration

Distance from headgate edge, ft	Laboratory		Intermediate		Final	
	Modulus, psi	Low stress, psi	Modulus, psi	Low stress, psi	Modulus, psi	Low stress, psi
18	8,493,000	-3,074	1,400,000	1,174	3,360,000	0.4
28	10,522,000	-9,029	770,000	1,056	1,800,000	-8.0
38	8,493,000	-6,200	920,000	1,144	2,100,000	-9.0
58	8,439,000	1,019	15,000,000	161	16,200,000	3.0
98	5,557,000	-8,608	430,000	979	950,000	-20.0
118	8,493,000	392	10,000,000	76	10,400,000	-7.0
178	10,522,000	-2,424	2,100,000	1,117	4,760,000	1.4
213	7,805,000	-4,807	890,000	1,044	2,100,000	20.0
248	5,681,000	8,534	360,000	921	880,000	.7

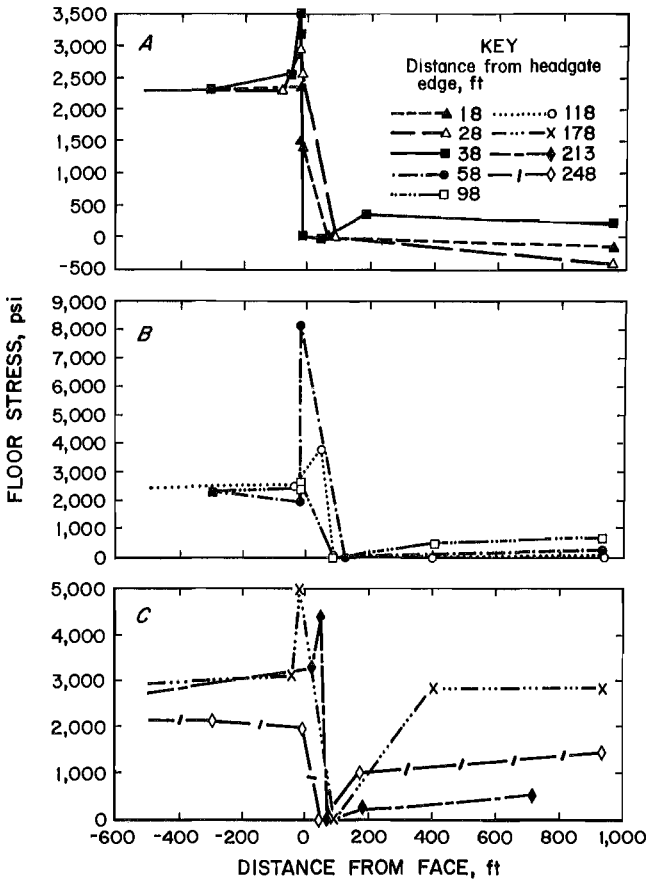

Figure 45.—Floor stress under headgate side of panel S-9 during panel S-9 mining. *A*, 18, 28, and 38 ft from headgate edge; *B*, 58, 98, and 118 ft from headgate edge; *C*, 178, 213, and 248 ft from headgate edge.

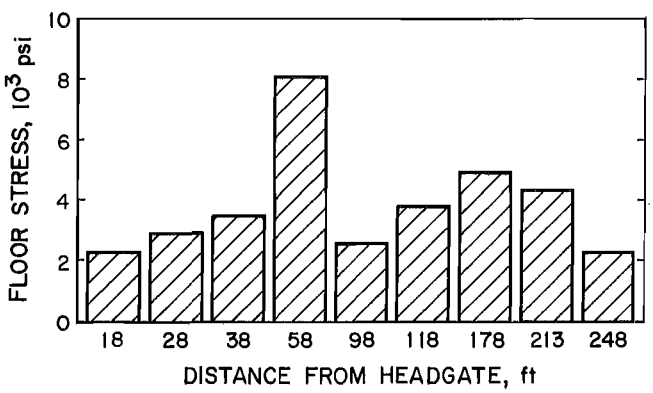

Figure 46.—Peak abutment stress for floor BPF's under panel S-9 during panel S-9 mining.

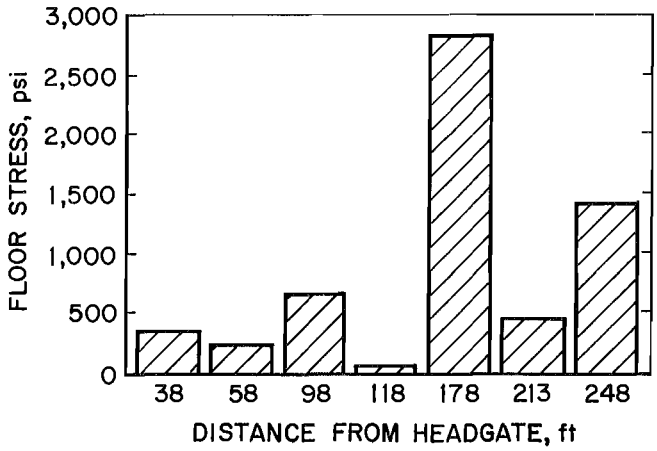

Figure 47.—Peak stress recovery for floor BPF's under panel S-9 during panel S-9 mining.

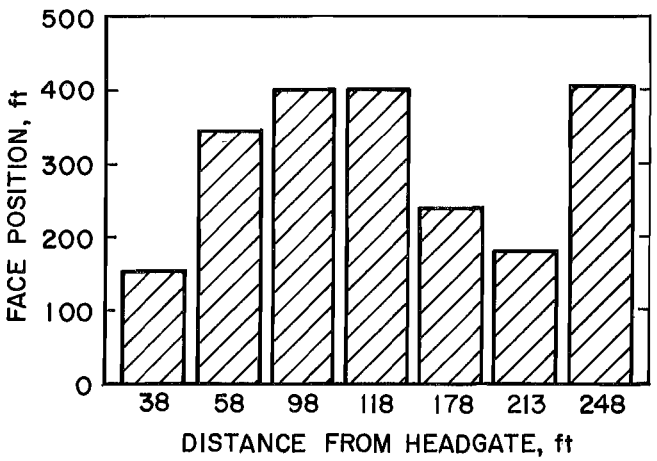

Figure 48.—Face position of panel S-9 mining at peak stress recovery for floor BPF's under panel S-9.

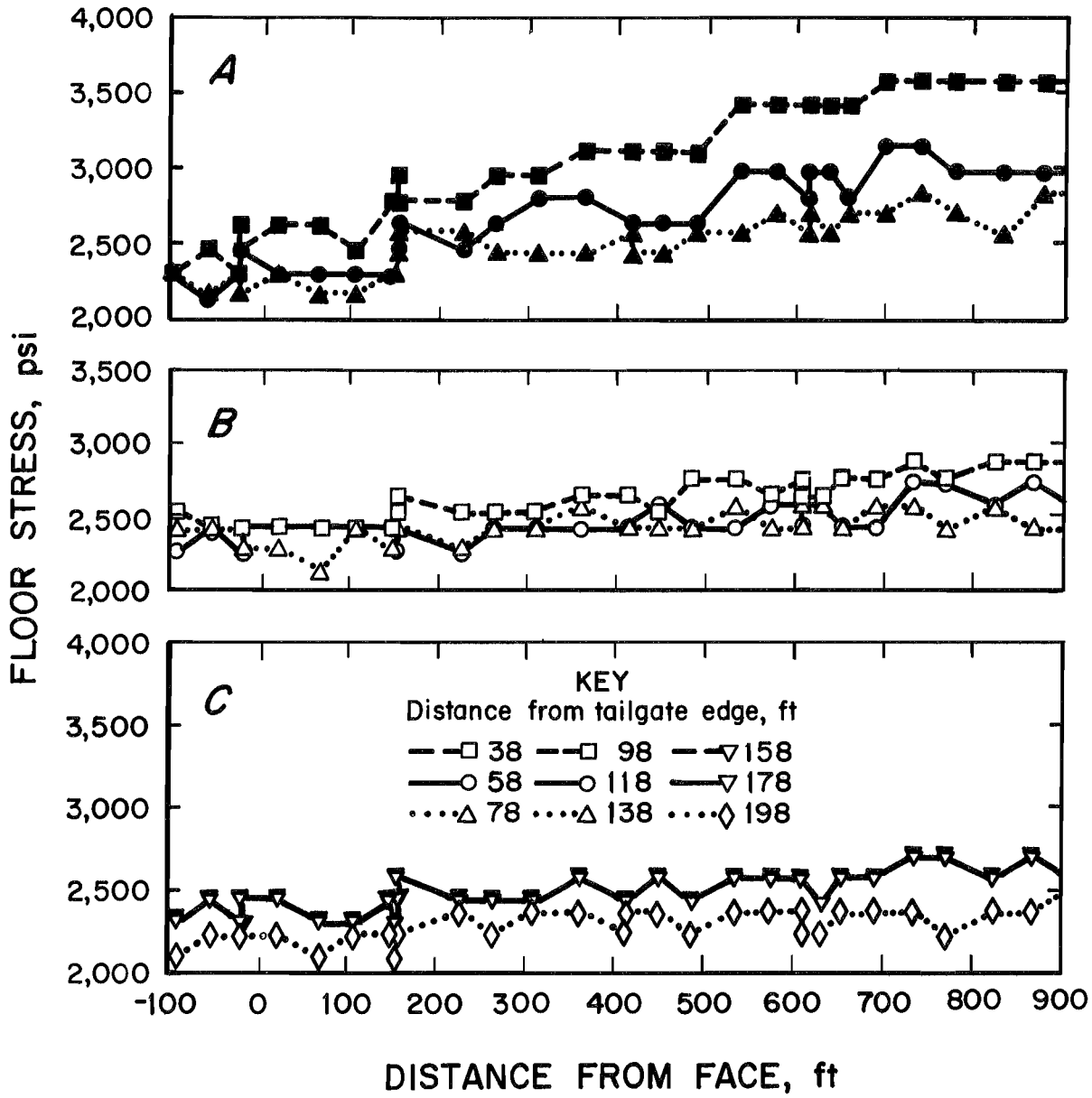

Figure 49.—Floor stress under tailgate side of panel S-10 during panel S-9 mining. *A*, 38, 58, and 78 ft from tailgate edge; *B*, 98, 118, and 138 ft from tailgate edge; *C*, 158, 178, and 198 ft from tailgate edge.

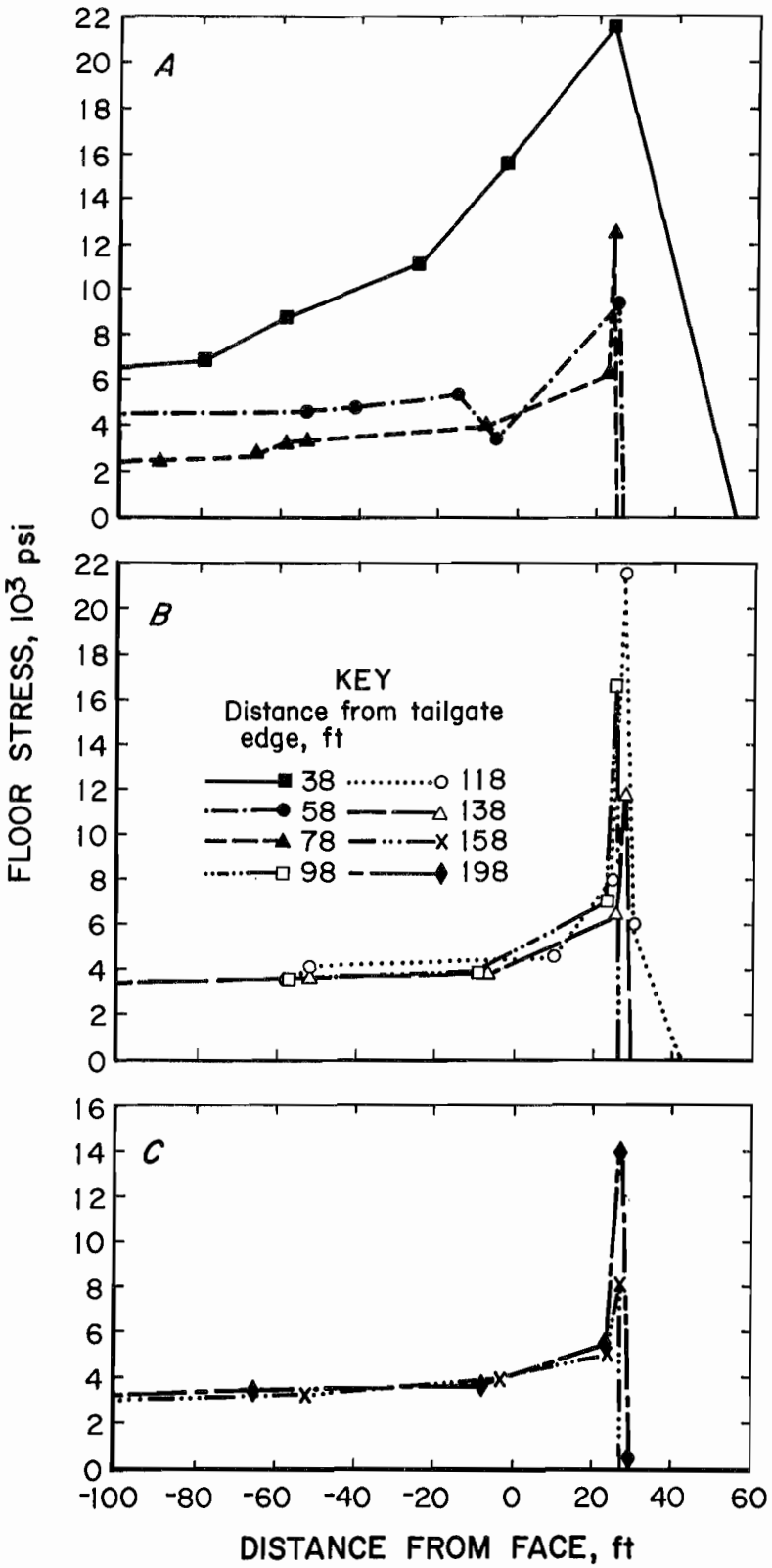

Figure 50.—Floor stress under tailgate side of panel S-10 during panel S-10 mining. *A*, 38, 58, and 78 ft from tailgate edge; *B*, 98, 118, and 138 ft from tailgate edge; *C*, 158 and 198 ft from tailgate edge.

edge, the mean and standard deviation of the peak front abutment stresses are 14,400 and 5,100 psi, respectively (fig. 51).

Comparison of figures 45 and 51 reveal that higher front abutment stress was measured on the tailgate side of panel S-10 as opposed to the headgate side of panel S-9. This reinforces coalbed stress change data reported by Campoli, Barton, Van Dyke, and Gauna (*3*), but must be viewed in light of the fact that the panel S-9 and S-10 data sets were calibrated with different BPFCAL procedures. Monitoring of floor stress BPF's was terminated by a roof fall in the 10 development gate-entry system. The data acquisition system trunk line was severed when mining of panel S-10 was 108 ft past the drill sump (fig. 21).

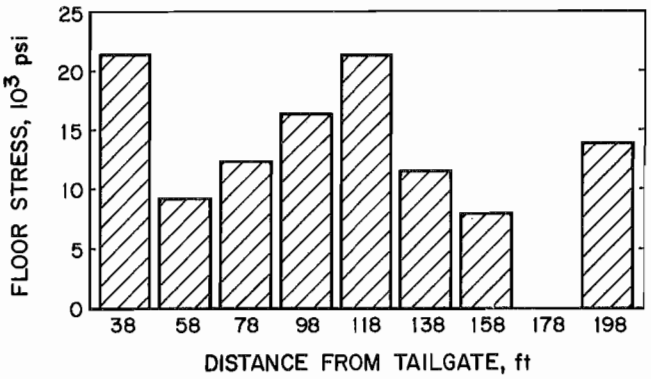

Figure 51.—Peak abutment stress for floor BPF's under panel S-10 during panel S-10 mining.

COMPOSITE STRESS DISTRIBUTION

Figure 52 is a composite summary of strata stress distribution across an adjacent longwall gob, tailgate abutment pillar, and currently mined longwall panel. It represents the strata stress when the mining of the longwall panel is within 20 ft of the composite instrumentation line. The panel S-9 floor stress data are employed under two scenarios, one representing the peak front abutment on the headgate side of the currently mined panel and the other representing the gob consolidation stress on the floor of the previously mined panel. The measured distributed stress shown by the crosshatched area of figure 52 is not equal to the original equilibrium pressure distribution as a result of the load not being applied symmetrical in three dimensions. When the face of the currently mined panel is within 20 ft of the composite instrumentation line, the three-dimensional environment consists of gob material behind the face and in the mined-out panel area that is imposing additional stress on the near-face portion of the currently mined panel. The measured stress on the currently mined panel of figure 52 above the original equilibrium pressure distribution comes from the load deficiency wedges formed by the gob of the currently mined and mined-out panels along with the load deficiency of the gate pillars. Furthermore, the percentages of measured load supported by the mined-out panel gob, tailgate pillars, and currently mined panel of figure 52 are 10%, 14%, and 76%, respectively.

Figure 53 is a composite summary of side abutment stress distribution across two half longwall panels and

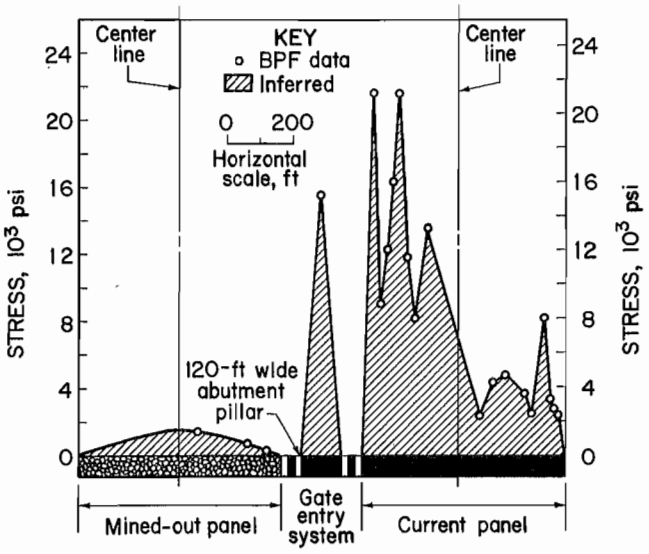

Figure 52.—Composite summary of strata stress distribution across adjacent longwall gob, tailgate abutment pillar, and currently mined longwall panel.

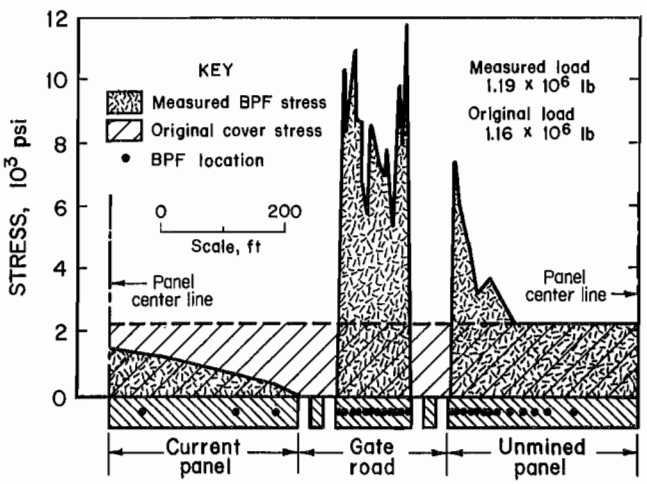

Figure 53.—Composite summary of side abutment stress distribution across two half longwall panels and headgate pillars.

headgate pillars when the face of the currently mined panel was greater than or equal to 500 ft beyond the composite instrumentation line. The measured stress shown in figure 53 is a compilation of BPF data documented in this report and by Campoli, Barton, Van Dyke, and Gauna (*3*) on this same mine working geometry. The measured BPF stress of figure 53 is almost exactly equal to the original equilibrium pressure distribution as a result of the load being applied symmetrical in three dimensions. This near equality helps confirm the accuracy of the measured stresses and stress distributions. Finally, the percentages of the measured load supported by the currently mined panel gob, headgate pillars, and unmined panel of figure 53 are 15%, 42%, and 43%, respectively.

SUMMARY AND CONCLUSIONS

Retreat longwall coal mining redistributes the natural stress state surrounding the mine openings. However, the sum total of the weight of the overburden remains unchanged. This redistribution of load requires a stress transfer so that a new equilibrium state can be achieved. The new equilibrium state is achieved when the weight of the overburden carried by the mined coal is redistributed among the longwall face, adjacent gob, active gob, gate road pillars, and adjacent unmined panel. The pattern of stress redistribution is controlled by the geologic setting.

The VP No. 3 Mine operator extracts the Pocahontas No. 3 Coalbed, which is located between rigid associated strata under approximately 2,100 ft of overburden. A previous field study in this mine documented a promising gate road design, which alleviated the risk of coal mine bumps on retreat longwall sections (*3*). To better understand why this gate road design was successful and to characterize longwall gob loading under bump-prone conditions, the gob load distribution was measured. The study area encompassed a conventionally designed gate road and the two adjacent 600- by 6,000-ft S-9 and S-10 longwall panels. The 238-ft-wide 10 development gate road consisted of 20- by 80-ft yield pillars on either side of 120- by 180-ft abutment pillars.

The performance of the 10 development gate road design during the mining of the S-9 and S-10 longwall panels was evaluated with an instrumentation array containing stainless steel BPF's for indicating changes in the abutment pillar stress; coal extensometers for measuring abutment pillar dilation, convergence stations for measuring roof-to-floor closure, and a differential roof-sag indicator for monitoring bedding separations in the immediate roof. The floor stress under a gate road abutment pillar, the headgate side of panel S-9, and the tailgate side of the S-10 panel was evaluated with specially designed stainless steel BPF's.

Minimal stress change was induced in the instrumented abutment pillar until the mining of panel S-9 reached the 600-ft face position. The effective bearing area of the 120- by 180-ft abutment pillar was reduced to a 60- by 130-ft rectangle at the 300-ft S-10 panel face position. At the 100-ft face position of panel S-10, only the geometric center of the abutment pillar continued to display a significant stress change value. Thus, it is concluded that after this point the entire pillar core was destroyed. The timing of this final destruction of the confined core is optimal since the abutment pillar is located between two gob areas and no longer of significant importance for strata control.

The pillar stress change and roof-to-floor entry convergence data are consistent in describing the mechanism and timing of abutment pillar high-stress behavior. An approximate convergence of 2.5 in and an approximate stress change of 6,000 psi were measured at the edge of the abutment pillar's confined core. Based on these values, the modulus of elasticity of the Pocahontas No. 3 Coalbed was estimated at 0.22 million psi. This realistic modulus of elasticity value lends credence to the use of convergence instrumentation to evaluate the mechanism and timing of subsequent gate road design variations. The relative proportionality between convergence and stress change was obtained as a result of the uniform behavior of the roof and floor.

A total of eighteen 3-in-diameter BPF's were installed in the floor rock below panels S-9 and S-10. The peak stress recovery under panel S-9 generally increases as distance from headgate edge increases. No measurable stress recovery occurred in the instruments 18 and 28 ft from the headgate edge of panel S-9. BPF's nearest the center of the panel rebounded to a value closest to the original cover stress of approximately 2,310 psi. The peak stress recovery generally occurred at the 400-ft face position (400 ft into the gob) of panel S-9 (0.2 times the overburden thickness). Panel S-9 gob floor stress was monitored during the remainder of panel S-9 mining and during panel S-10 mining without significant stress change from that measured at the 400-ft face position of panel S-9.

The panel S-9 mining caused noticeable side abutment stress in the BPF's 38, 58, and 78 ft from the tailgate edge of panel S-10. However, the BPF's closer to the panel center appeared to record values only slightly greater than original cover stress while decreasing in magnitude as their BPF location got closer to panel center. Stress did not again increase in the BPF's below panel S-10 until its mining was within 100 ft of the instrument line. The floor

stress dramatically increased to peak front abutment stress when the face was within 20 ft of the instrument line. The peak front abutment across the tailgate side of panel S-10 occurred at 38 and 118 ft from the tailgate edge.

It is concluded that the majority of the stress is concentrated on the currently mined panel and on the 120-ft-wide abutment pillar, with the smallest portion of the stress carried by the gob of the previously mined panel. Furthermore, a significantly greater portion of the peak front abutment stress is supported by the tailgate side of the currently mined panel than by the headgate side. Thus, the magnitude of peak front abutment stress on the tailgate side of the currently mined panel, coupled with the time of failure of the abutment pillar in the adjacent gate road, control longwall face bumps. Therefore, strengthening the abutment pillar can delay failure until it is between two gob areas, mitigating longwall face bumps.

REFERENCES

1. Babcock, C. O. Equations for the Analysis of Borehole Pressure Cell Data. Paper in 27th Symposium on Rock Mechanics. Univ. AL, Tuscaloosa, AL, 1986, pp. 233-241.

2. Barton, T. M., and A. A. Campoli. Rock Mechanics Research Decreases Longwall Bump Potential. Soc. Min. Eng. AIME preprint 91-79, 1991, 6 pp.

3. Campoli, A. A., T. M. Barton, F. C. Van Dyke, and M. Gauna. Mitigating Destructive Longwall Bumps Through Conventional Gate Entry Design. BuMines RI 9325, 1990, 38 pp.

4. Campoli, A. A., and K. A. Heasley. Coal Mine Bump Research: Providing Tools for Rational Longwall Design. Paper in Proceedings of the 23rd International Conference of Safety in Mines Research Institutes, Washington, DC, Sept. 11-15, 1989. BuMines OFR 27-89, 1989, pp. 666-676.

5. Campoli, A. A., C. A. Kertis, and C. A. Goode. Coal Mine Bumps: Five Case Studies in the Eastern United States. BuMines IC 9149, 1987, 34 pp.

6. Campoli, A. A., D. C. Oyler, and F. E. Chase. Performance of a Novel Bump Control Pillar Extracting Technique During Room-and-Pillar Retreat Coal Mining. BuMines RI 9240, 1989, 40 pp.

7. Condon, J. L., and R. D. Munson. Microseismic Monitoring of Mountain Bumps and Bounces: A Case Study. Paper in Proceedings of the 6th International Conference on Ground Control in Mining. WV Univ., Morgantown, WV, 1987, pp. 1-9.

8. Ferm, J. C., and G. A. Weisenfluh. Cored Rocks of the Southern Appalachian Coal Fields. Univ. KY, Lexington, KY, 1981, 112 pp.

9. Heasley, K. A. An Examination of Energy Calculations Applied to Coal Bump Prediction. Paper in Proceedings of the 10th International Conference on Ground Control in Mining (Morgantown, WV, June 10-12, 1991). WV Univ., Coll. Miner. and Eng. Resour., 1991, pp. 122-129.

10. ___. Understanding the Hydraulic Pressure Cell. Paper in Rock Mechanics as a Guide for Efficient Utilization of Natural Resources, ed. by A. W. Khair (Proc. 30th U.S. Symp. on Rock Mech., Morgantown, WV, June 18-23, 1989). Balkema, 1989, pp. 485-492.

11. Holland, C. T., and E. Thomas. Coal-Mine Bumps: Some Aspects of Occurrence, Cause, and Control. BuMines B 535, 1954, 37 pp.

12. Hsuing, S. M., and S. S. Peng. Chain Pillar Design for U.S. Longwall Panels. Min. Sci. and Technol., v. 2, 1985, pp. 279-305.

13. Iannacchione, A. T. Behavior of a Coal Pillar Prone To Burst in the Southern Appalachian Basin of the United States. Paper in Pre-Printed Papers (2d Int. Symp. Rockbursts and Seismicity in Mines, Minneapolis, MN, June 8-10, 1988). Univ. MN, Minneapolis, MN, 1988, pp. 427-439.

14. Iannacchione, A. T. Numerical Simulation of Coal Pillar Loading With the Aid of a Strain-Softening Finite Difference Model. Paper in Rock Mechanics as a Guide for Efficient Utilization of Natural Resources (Proc. 30th U.S. Symp. on Rock Mech., Morgantown, WV, June 18-23, 1989). Balkema, 1989, pp. 775-782.

15. Iannacchione, A. T., A. A. Campoli, and D. C. Oyler. Fundamental Studies of Coal Mine Bumps in the Eastern United States. Paper in Rock Mechanics, ed. by I. Farmer, J. J. K. Daemen, C. S. Desai, C. E. Glass, and S. P. Newman. Balkema, 1987, pp. 1063-1072.

16. King, H. J., and B. N. Whittaker. A Review of Current Roadway Behavior. Paper in the Proceedings of the Symposium on Roadway Strata Control. Inst. Min. and Metall., 1971, pp. 73-87.

17. Kripakov, N. P., L. A. Beckett, D. A. Donato, and J. S. Durr. Computer-Assisted Mine Design Procedures for Longwall Mining. BuMines RI 9172, 1988, 38 pp.

18. Mark, C. Pillar Design Methods for Longwall Mining. BuMines IC 9247, 1990, 53 pp.

19. Oyanguren, P. R. Simultaneous Extraction of Two Potash Beds in Close Proximity. Ch. 32 in Proceedings of the 5th International Strata Control Conference. 1972, 5 pp.

20. Park, D. W., and V. Gall. Supercomputer Assisted Three-Dimensional Finite Element Analysis of a Longwall Panel. Paper in Rock Mechanics as a Guide for Efficient Utilization of Natural Resources: Proceedings of the 30th U.S. Symposium. Balkema, 1989, pp. 133-140.

21. Peng, S. S., and H. S. Chiang. Longwall Mining. Wiley, 1984, 708 pp.

22. Rice, G. S. Bumps in Coal Mines of the Cumberland Field, Kentucky and Virginia—Causes and Remedy. BuMines RI 3267, 1935, 36 pp.

23. Talman, W. G., and J. L. Schroder, Jr. Control of Mountain Bumps in the Pocahontas No. 4 Seam. Trans. AIME, 1958, pp. 888-891.

24. Wade, L. V., and P. J. Conroy. Rock Mechanics Study of a Longwall Panel. Min. Eng., v. 268, Dec. 1980, pp. 1728-1734.

25. Wang, F. -D., W. A. Skelly, and J. Wolgamott. In-Situ Coal Pillar Strength Study (contract H0242022, CO Sch. Mines). BuMines OFR 107-79, 1976, 243 pp.

26. Wilson, A. H. A Hypothesis Concerning Pillar Stability. Min. Eng. (London), v. 131, 1973, pp. 409-417.

27. ___. Pillar Stability in Longwall Mining. State-of-the-Art of Ground Control in Longwall Mining and Mining Subsidence. AIME, , 1982, pp. 85-95.

INT.BU.OF MINES,PGH.,PA 29681

USGPO: 1993--709-008/60102